Charming New B-Physics

Sebastian Jäger, ^{a} Matthew Kirk,^{b} Alexander Lenz^c and Kirsten Leslie^a

^{a}*University of Sussex, Department of Physics and Astronomy, Falmer, Brighton BN1 9QH, UK*

^{b}*Dipartimento di Fisica, Università di Roma "La Sapienza" & INFN Sezione di Roma, Piazzale Aldo Moro 2, 00185 Roma, Italy*

^{c}*IPPP, Department of Physics, Durham University, Durham DH1 3LE, UK*

E-mail: S.Jaeger@sussex.ac.uk, matthew.kirk@roma1.infn.it, alexander.lenz@durham.ac.uk, k.leslie@sussex.ac.uk

Abstract: We give a comprehensive account of the flavour physics of Beyond-Standard-Model (BSM) effects in $b \to c\bar{c}s$ transitions, considering the full set of 20 four-quark operators. We discuss the leading-order structure of their RG mixing with each other as well as the QCD-penguin, dipole, and FCNC semileptonic operators they necessarily mix with, providing compact expressions. We also provide the first complete results for BSM effects in the lifetime observables $\Delta\Gamma_s$ and $\tau(B_s)/\tau(B_d)$, as well as for the semileptonic CP-asymmetry a_{sl}^s. From a global analysis, we obtain stringent constraints on 16 of the 20 BSM operators, including the 10 operators $Q_{1\ldots10}^{c'}$ involving a right-handed strange quark. Focussing on CP-conserving new physics, the constraints correspond to NP scales of order 10 TeV in most cases, always dominated by exclusive and/or radiative B-decays via RGE mixing. For the remaining four operators, including the two Standard-Model (SM) ones, larger effects are experimentally allowed, as previously noted in [1]. We extend that paper's scope to the CP-violating case, paying attention to the impact on the decay rate and time-dependent CP-violation in $B_d \to J/\psi K_S$. Contrary to common lore, we show that quantifiable constraints arise for new physics in either of the two SM operators, with the uncertain non-perturbative matrix element of the colour-suppressed (or equivalently, colour-octet) operator determined from the data. For new physics in the coefficient C_1^c, suppressed in the SM, we find (in addition to CP-conserving new physics) two perfectly viable, narrow bands of complex Wilson coefficients. Somewhat curiously, one of them contains a region where the fitted matrix element for the colour-suppressed operator is in agreement with naive factorization, contrarily to a widely held belief that large non-factorizable contributions to $B_d \to J/\psi K_S$ are implied by experimental data.

Contents

1 Introduction

A wide range of B meson decays are affected by $b \to c\bar{c}s$ transitions, providing the opportunity to use a rich set of complementary observables to detect possible new physics (NP), or place constraints on such dynamics and its mass scale. These partonic transitions are generated at the tree level in the SM, and contribute again at tree level to lifetime observables such as $\Delta\Gamma_s$ and $\tau(B_s)/\tau(B_d)$ [2], which stand out among others through their good theoretical control. Moreover, as we have shown in [1], there is the possibility that

operators with this flavour structure can be involved in the rare B-decay anomalies [3–14][1]. In this case, the contribution to the observables is through a charm loop, which radiatively generates the semileptonic Wilson coefficient C_{9V}, conjectured to lie behind the so-called P_5' anomaly.[2] That BSM $b \to c\bar{c}s$ transitions can give important one-loop contributions to rare radiative and semileptonic decays should not really be surprising, given the same happens in the SM, where charm loops provide on the order of one-half of the $b \to s\gamma$ decay amplitude, as well as of C_{9V}. The size of these effects is amplified by strong renormalization-group (RG) running in the SM, which can be even stronger for certain BSM operators [1]. Neither does the NP scale need to be particularly low: because of strong RGE running, accounting for the P_5' anomaly merely requires a BSM contribution $|C_1^{\mathrm{BSM}}| \sim 0.1$, giving a naive NP scale

$$\Lambda_{\mathrm{NP}} \sim \left(\frac{4\,G_F}{\sqrt{2}} |V_{cs}^* V_{cb}| \times 0.1 \right)^{-1/2} \sim 3\,\mathrm{TeV}\,.$$

For a weakly coupled, sufficiently leptophobic tree-level mediator, this may be allowed by high-p_T LHC searches, and will not cause problems with electroweak precision observables. For strong coupling, the NP scale can be as high as $30\,\mathrm{TeV}$ and out of the reach of LHC direct searches altogether [1].

A BSM model that generates new physics only in $b \to c\bar{c}s$ is not realistic, as is already evident from the leading-order RG mixing we have mentioned. Thus the model-independent study presented here has to be considered as a building block in constructing or constraining UV models.

In the present paper, we extend the analysis of [1] in the following ways:

- We study a full basis of 20 $b \to c\bar{c}s$ operators, where [1] focused on those 4 that can generate the P_5' anomaly, and we obtain stringent constraints on the 16 others.

- We extend the case of C_{1-4}^c to allow for CP-violating NP and show how to include $B_d \to J/\psi K_S$ data with minimal non-perturbative inputs.

To address the first item, we build the anomalous dimension matrix governing the RG evolution of the 34 relevant operators, and review the all-order block structure. We explain that, while some blocks first arise at one-loop order and others at two-loop order, an unambiguous leading-order evolution operator arises, and obtain a compact numerical expression for it. This can be useful in understanding how different four-quark operator coefficients affect the rare and semileptonic decays, but may also be useful to a reader wishing to consider a particular UV model, particularly when multi-operator correlations are important that go beyond the one- and two-parameter cases we consider in our model-independent phenomenology.

We also compute the complete BSM contribution to the $\Delta B = 0$ and $\Delta B = 2$ lifetime observables, including the impact on the semileptonic CP asymmetry a_{sl}^s.

---

[1]The possibility of virtual charm BSM physics in rare semileptonic decay was raised in [15]

[2] As a peculiar feature, this mechanism can induce a q^2-dependent BSM contribution to C_{9V}. Such a q^2 dependence, should it be implied by future experimental data, might otherwise have been taken as an unambiguous sign for a hadronic origin of the anomaly.

Regarding the second item, a key point is that once CP violation is switched on, contributions to time-dependent CP violation in $B_d \to J/\psi K_S$ are generated, the sine coefficient of which is precisely measured and usually taken to provide a clean determination of the CKM angle β; this no longer holds in the present context. However, we find that as long as NP only affects one of the two Wilson coefficients present in the SM, the global data set is sufficient to determine the (complex) ratio of the two relevant non-perturbative matrix elements jointly with the complex Wilson coefficient, such that theory input is needed only for the matrix element of the operator Q_1^c, which on grounds of large-N arguments alone should be close to its naive-factorization value (as is also borne out by QCD factorization, even though QCDF is not expected to provide reliable quantitative results).

As phenomenological results, for the 16 operators not previously considered we provide constraints for the CP-conserving case, almost all of which turn out to be of order 10 TeV. In addition, we discuss in detail the constraints on the two one-parameter CP-violating scenarios where we have a complex BSM contribution to one of the two SM coefficients $C_{1,2}^c$. As a perhaps curious result, we find that among the allowed regions is one where CP-violating BSM affects C_1 in such a way that the matrix element of Q_2^c is *also* close to its naive-factorization value.

We note that BSM effects in hadronic tree-level decays have previously been systematically studied in [16, 17]. In these works all hadronic decay channels of the b quark were considered and the new contributions to the Wilson coefficients were also allowed to be complex, but only the SM operators Q_1^c and Q_2^c were investigated.

The layout of our paper is as follows: In Section 2 we describe the setup of our model, specifying our operator basis and giving the RG evolution. Section 3 is devoted to our theoretical results for the lifetime observables, radiative and rare decay contributions, as well as our approach to $B_d \to J/\psi K_S$, and constitutes one of two main parts of our paper. As the second main part, we describe our phenomenological constraints in Section 4 (details of the inputs we use are is given in Section 4.1). Our conclusions can be found in Section 5.

2 Setup

2.1 Operator basis

For our study of BSM $b \to c\bar{c}s$ effects we use the following weak effective Hamiltonian

$$\mathcal{H}_{\text{eff}} = \mathcal{H}_{\text{eff}}^{c\bar{c}} + \mathcal{H}_{\text{eff}}^{rsl} + \mathcal{H}_{\text{eff}}^{QCD} \, . \tag{2.1}$$

The first part $\mathcal{H}_{\text{eff}}^{c\bar{c}}$ contains a complete set of 20 $b \to c\bar{c}s$ four-fermion operators, reading

$$\mathcal{H}_{\text{eff}}^{c\bar{c}} = \frac{4G_F}{\sqrt{2}} \lambda_c \sum_{i=1}^{10} \left[C_i^c(\mu) Q_i^c(\mu) + C_i^{c\prime}(\mu) Q_i^{c\prime}(\mu) \right] + \text{h.c.} \, . \tag{2.2}$$

Here $\lambda_p = V_{pb}V_{ps}^*$ for $p = u, c, t$ are CKM structures, and the Wilson coefficients $C_i^{c(\prime)}$ and operators $Q_i^{c(\prime)}$ are renormalized at the scale μ. The operators Q_i^c read

$$Q_1^c = (\bar{c}_L^i \gamma_\mu b_L^j)(\bar{s}_L^j \gamma^\mu c_L^i), \qquad Q_2^c = (\bar{c}_L^i \gamma_\mu b_L^j)(\bar{s}_L^j \gamma^\mu c_L^j),$$

$$Q_3^c = (\bar{c}_R^i b_L^j)(\bar{s}_L^j c_R^i), \qquad Q_4^c = (\bar{c}_R^i b_L^i)(\bar{s}_L^j c_R^j),$$

$$Q_5^c = (\bar{c}_R^i \gamma_\mu b_R^j)(\bar{s}_L^j \gamma^\mu c_L^i), \qquad Q_6^c = (\bar{c}_R^i \gamma_\mu b_R^i)(\bar{s}_L^j \gamma^\mu c_L^j),$$

$$Q_7^c = (\bar{c}_L^i b_R^j)(\bar{s}_L^j c_R^i), \qquad Q_8^c = (\bar{c}_L^i b_R^i)(\bar{s}_L^j c_R^j),$$

$$Q_9^c = (\bar{c}_L^i \sigma_{\mu\nu} b_R^j)(\bar{s}_L^j \sigma^{\mu\nu} c_R^i), \qquad Q_{10}^c = (\bar{c}_L^i \sigma_{\mu\nu} b_R^i)(\bar{s}_L^j \sigma^{\mu\nu} c_R^j), \tag{2.3}$$

where i, j are $SU(3)$ colour indices and $\psi_{L,R}$ denotes the projections $\psi_{L,R} = (1 \mp \gamma^5)/2 \cdot \psi$. The remaining 10 operators $Q_i^{c\prime}$ are obtained from those displayed by letting $L/R \to R/L$. In the SM the operators Q_1^c and Q_2^c arise due to a tree-level W exchange. All other 18 operators are genuine BSM effects. For the overall normalisation of these operators we have chosen the CKM normalisation of the SM operators, which contains a tiny imaginary part.

For radiative and semileptonic decays $b \to s\gamma$ and $b \to s\ell^+\ell^-$, further operators contribute. These comprise the radiative and semileptonic operators

$$Q_{7\gamma} = \frac{em_b}{16\pi^2}(\bar{s}_L \sigma_{\mu\nu} b_R) F^{\mu\nu}, \qquad Q_{9V} = \frac{\alpha}{4\pi}(\bar{s}_L \gamma_\mu b_L)(\bar{\ell}\gamma^\mu \ell), \tag{2.4}$$

and their parity conjugates, again denoted by primes. m_b denotes the $\overline{\text{MS}}$ b-quark mass, e is the electromagnetic coupling, and $\alpha = \frac{e^2}{4\pi}$. These operators enter through the second part $\mathcal{H}_{\text{eff}}^{rsl}$ of (2.1)

$$\mathcal{H}_{\text{eff}}^{rsl} = -\frac{4G_F}{\sqrt{2}}\lambda_t \left[C_{7\gamma}(\mu)Q_{7\gamma}(\mu) + C_{9V}(\mu)Q_{9V}(\mu) + C'_{7\gamma}(\mu)Q'_{7\gamma}(\mu) + C'_{9V}(\mu)Q'_{9V}(\mu) \right] + \text{h.c.} . \tag{2.5}$$

Moreover, they receive contributions from QCD penguin operators, contained in the third term $\mathcal{H}_{\text{eff}}^{QCD}$ of (2.1),

$$\mathcal{H}_{\text{eff}}^{QCD} = -\frac{4G_F}{\sqrt{2}}\lambda_t \left\{ \sum_{i=3}^{6} \left[C_i^p(\mu)P_i(\mu) + C_i^{p\prime}(\mu)P'_i(\mu) \right] + C_{8g}(\mu)Q_{8g}(\mu) + C'_{8g}(\mu)Q'_{8g}(\mu) \right\} . \tag{2.6}$$

Our QCD penguin operators are defined in [18] and include the chromomagnetic dipole operator, reading explicitly:

$$P_3 = (\bar{s}_L \gamma_\mu b_L) \sum_q (\bar{q}\gamma^\mu q), \qquad P_4 = (\bar{s}_L \gamma_\mu T^a b_L) \sum_q (\bar{q}\gamma^\mu T^a q),$$

$$P_5 = (\bar{s}_L \gamma_\nu \gamma_\mu \gamma_\rho b_L) \sum_q (\bar{q}\gamma^\nu \gamma^\mu \gamma^\rho q), \qquad P_6 = (\bar{s}_L \gamma_\nu \gamma_\mu \gamma_\rho T^a b_L) \sum_q (\bar{q}\gamma^\nu \gamma^\mu \gamma^\rho T^a q),$$

$$Q_{8g} = \frac{g_s m_b}{16\pi^2}(\bar{s}\sigma^{\mu\nu} T^a P_R b) G_{\mu\nu}^a, \tag{2.7}$$

where q runs over all active quark flavours in the effective theory, i.e. $q = u, d, s, c, b$, and a prime again denotes a chirality conjugate. Our complete operator basis comprises

34 operators and closes under QCD renormalization. We renormalize our operators as in [18–21]. We will neglect the tiny contribution $|\lambda_u| \approx 0.00084$[3] [22] (for similar results see [23]) and we thus get from unitarity of the CKM matrix $\lambda_c = -\lambda_t$.

To isolate the BSM contribution, we split the Wilson coefficients into SM parts and BSM parts,

$$C_i^c(\mu) = C_i^{\mathrm{SM}}(\mu) + \Delta C_i(\mu)\,. \tag{2.8}$$

We will neglect the small mass ratios m_q/m_W and m_s/m_b, which implies the vanishing of all primed Wilson coefficients in the SM, $C_i'^{,\mathrm{SM}}(\mu) = 0$ and in addition the vanishing of the four-quark coefficients $C_i^{c,\mathrm{SM}}(\mu) = 0$ for $i \neq 2$. For our phenomenology we will also assume that at an input scale $\mu_0 \sim M_W$, the ΔC_i vanishes for all but the four-quark operators. This corresponds to what we called 'Charming Beyond the Standard Model' (CBSM) scenario in [1]. As described below, RG evolution then generates BSM contributions to the penguin and dipole operators, which play a crucial role in the phenomenology of the CBSM scenario. The CBSM scenario should be viewed as a partial effective description of a more complete UV scenario, which will in general also involve nonzero initial values for the other ΔC_i.

2.2 Renormalization-group evolution

As emphasized in our previous work [1], operator mixing can have a dramatic impact on the radiative and semileptonic Wilson coefficients, and as a result on the contributions of the $b \to c\bar{c}s$ operators to the radiative and rare semileptonic decays. It is therefore crucial to include its effects, which is conveniently done through renormalization-group evolution from the BSM scale μ_0 where the Wilson coefficients are initially obtained to a scale $\mu \sim m_b$ appropriate to evaluating B-physics observables.

Collecting the 17 unprimed Wilson coefficients into a vector $\vec{C}$, the coupled system of renormalization-group equations (RGE) governing their dependence on the renormalization scale μ can be written in matrix notation as

$$\mu \frac{d}{d\mu} \vec{C}(\mu) = \gamma^T(\mu) \vec{C}(\mu)\,, \tag{2.9}$$

where γ is the anomalous-dimension matrix. Note that the unprimed and primed Wilson coefficients do not mix at any order in QCD; moreover, the 17 primed Wilson coefficients, collectively denoted $\vec{C}'$, fulfil the same set of equations (2.9), with identical anomalous-dimension matrix. Both statements follow directly from the parity invariance of QCD. The solution of (2.9) is a linear relation

$$\vec{C}(\mu) = U(\mu, \mu_0) \vec{C}(\mu_0) \tag{2.10}$$

in terms of the so-called evolution operator $U(\mu, \mu_0)$, which itself satisfies (2.9). Importantly, the SM and BSM parts $\vec{C}^{\mathrm{SM}}$ and $\Delta\vec{C}$ separately satisfy (2.10).

---

[3]Considering CP violating observables this approximation might be violated, since $\Im(\lambda_u)$ is of a similar size as $\Im(\lambda_{c,t})$, see the discussion at the end of Section 3.2.

If the leading-order anomalous-dimension matrix has the form

$$\gamma(\mu) = \frac{\alpha_s(\mu)}{4\pi} \gamma^{(0)} \, , \qquad (2.11)$$

where $\gamma^{(0)}$ is a constant matrix, then the explicit form of the evolution operator to leading logarithmic order is

$$U^{(0)}(\mu, \mu_0) = \exp\left[-\frac{(\gamma^{(0)})^T}{2\beta_0} \ln\left(\frac{\alpha_s(\mu)}{\alpha_s(\mu_0)} \right) \right] \, , \qquad (2.12)$$

where β_0 is the leading coefficient in the QCD β-function,

$$\beta(\alpha_s) = \mu \frac{d\alpha_s}{d\mu} = -2\beta_0 \frac{\alpha_s^2}{4\pi} + \ldots \, . \qquad (2.13)$$

In the CBSM setup, two sources of complication arise. The first is that the leading-order anomalous-dimension matrix does not have the form (2.11). The second is that part of the anomalous-dimension matrix first arises at 2-loop order. To discuss both issues further, let us decompose the Wilson coefficient vector $\vec{C}$ into subcomponents,

$$\vec{C}(\mu) = (\vec{C}^c(\mu), \vec{C}^p(\mu), C_{8g}(\mu), C_{7\gamma}(\mu), C_{9V}(\mu)). \qquad (2.14)$$

The anomalous-dimension matrix then has the block form

$$\gamma = \begin{pmatrix} \hat{\gamma}_{cc} & \hat{\gamma}_{cp} & \vec{\gamma}_{c8} & \vec{\gamma}_{c7} & \vec{\gamma}_{c9} \\ 0 & \hat{\gamma}_{pp} & \vec{\gamma}_{p8} & \vec{\gamma}_{p7} & \vec{\gamma}_{p9} \\ 0 & 0 & \gamma_{88} & \gamma_{87} & 0 \\ 0 & 0 & 0 & \gamma_{77} & 0 \\ 0 & 0 & 0 & 0 & \gamma_{99} \end{pmatrix} \, , \qquad (2.15)$$

which holds to all orders of QCD.[4] The element γ_{99} vanishes for our normalization of Q_{9V}, which makes it proportional to a conserved quark current, but we will consider a different normalization shortly. γ_{77}, γ_{88}, $\vec{\gamma}_{cp}$, and $\hat{\gamma}_{cc}$ first arise at one-loop order, giving rise to the form (2.11) at leading order. $\vec{\gamma}_{p7}$ and $\vec{\gamma}_{p8}$ arises first at two-loop order. This makes them scheme-dependent already at leading order, though the explicit coupling factors in the definitions of $Q_{7\gamma}$ and Q_{8g} imply that the form (2.11) is maintained. On the other hand, some of the elements of $\vec{\gamma}_{c7}$, $\vec{\gamma}_{c8}$, $\vec{\gamma}_{c9}$ and $\vec{\gamma}_{p9}$ are non-zero at one loop, but with no accompanying factor of α_s.

To make this more explicit, let us decompose the set of $(\bar{c}b)(\bar{s}c)$ Wilson coefficients further, $\vec{C} = (\vec{C}_{1\ldots6}, \vec{C}_{7\ldots10}) \equiv (\vec{C}_A, \vec{C}_B)$, and further decompose the anomalous dimension

---

[4]The $(7c)$, $(8c)$, $(7p)$, $(8p)$, (79), and (89) entries vanish in a massless scheme due to the different dimensionality of the dipole and four-fermion operators, the (pc) block because of the flavour symmetries of massless QCD.

accordingly,

$$\gamma = \begin{pmatrix} \hat{\gamma}_{AA} & 0 & \hat{\gamma}_{Ap} & \vec{\gamma}_{A8} & \vec{\gamma}_{A7} & \vec{\gamma}_{A9} \\ 0 & \hat{\gamma}_{BB} & 0 & \vec{\gamma}_{B8} & \vec{\gamma}_{B7} & 0 \\ 0 & 0 & \hat{\gamma}_{pp} & \vec{\gamma}_{p8} & \vec{\gamma}_{p7} & \vec{\gamma}_{p9} \\ 0 & 0 & 0 & \gamma_{88} & \gamma_{87} & 0 \\ 0 & 0 & 0 & 0 & \gamma_{77} & 0 \\ 0 & 0 & 0 & 0 & 0 & \gamma_{99} \end{pmatrix} \overset{\text{LO}}{\sim} \begin{pmatrix} \frac{\alpha_s}{4\pi} & 0 & \frac{\alpha_s}{4\pi} & \frac{\alpha_s}{4\pi} & \frac{\alpha_s}{4\pi} & 1 \\ 0 & \frac{\alpha_s}{4\pi} & 0 & 1 & 1 & 0 \\ 0 & 0 & \frac{\alpha_s}{4\pi} & \frac{\alpha_s}{4\pi} & \frac{\alpha_s}{4\pi} & \frac{\alpha_s}{4\pi} \\ 0 & 0 & 0 & \frac{\alpha_s}{4\pi} & \frac{\alpha_s}{4\pi} & 0 \\ 0 & 0 & 0 & 0 & \frac{\alpha_s}{4\pi} & 0 \\ 0 & 0 & 0 & 0 & 0 & \frac{\alpha_s}{4\pi} \end{pmatrix}. \tag{2.16}$$

In the second expression we have indicated in what blocks factors of $\alpha_s/(4\pi)$ do or do not arise at leading order. The loop- and coupling-order of the leading contributions to each block are also given in Table 1 (the full algebraic expressions for each block are given in Appendix A). In (2.16) we have also made explicit which blocks vanish to all orders in QCD. Besides those blocks whose vanishing is already expressed through (2.15), these are the blocks concerning the would-be mixing of the four-quark operators in class B, i.e. $Q^c_{7...10}$, with the QCD penguin operators and Q_{9V}.[5] As a result of the structure of (2.16), $\vec{C}_A$ and $\vec{C}_B$ do not mix; their renormalization, including the mixing of each into the QCD penguins, dipoles, and C_{9V}, can therefore be considered independently. The evolution in the situation where only one of $\vec{C}_A$ or $\vec{C}_B$ is present is described by an anomalous dimension of the form (2.15), with $\hat{\gamma}_{cc} \to \gamma_{XX}$, $\hat{\gamma}_{cp} \to \hat{\gamma}_{Xp}$, $\vec{\gamma}_{c8} \to \vec{\gamma}_{X8}$, $\vec{\gamma}_{c7} \to \vec{\gamma}_{X7}$, and $\vec{\gamma}_{c9} \to \vec{\gamma}_{X9}$, where $X = A$ or B as applicable; let us refer to these limiting cases as 'case A' and 'case B', respectively.

Block	Loop Order	Coupling Order
$\hat{\gamma}_{AA}, \hat{\gamma}_{BB}, \hat{\gamma}_{Ap}, \hat{\gamma}_{pp}$ $\gamma_{77}, \gamma_{87}, \gamma_{88}, \vec{\gamma}_{p9}$	1	$\alpha_s^{(1)}$
$\vec{\gamma}_{A7}, \vec{\gamma}_{A8}, \vec{\gamma}_{p7}, \vec{\gamma}_{p8}$	2	$\alpha_s^{(1)}$
$\vec{\gamma}_{B7}, \vec{\gamma}_{B8}, \vec{\gamma}_{A9}$	1	$\alpha_s^{(0)}$

Table 1

Let us first consider case A, which includes the subset of operators discussed in [1] and in particular includes the SM case. Here, a rescaling

$$Q_{9V}(\mu) = \frac{\alpha_s(\mu)}{4\pi} \tilde{Q}_{9V}(\mu), \qquad C_{9V}(\mu) = \frac{4\pi}{\alpha_s(\mu)} \tilde{C}_{9V}(\mu), \tag{2.17}$$

is sufficient to bring the anomalous-dimension matrix into the form (2.11), such that the solution (2.12) applies (note that with the rescaling, $\gamma_{99} \to -2\beta_0$). This also shows that C_{9V} formally starts at order $1/\alpha_s$ when $\vec{C}_A$ is nonzero (which includes the SM case). The blocks $\vec{\gamma}_{A7}, \vec{\gamma}_{A8}, \vec{\gamma}_{p7}$, and $\vec{\gamma}_{p8}$, due to two-loop diagrams, are scheme-dependent and induce

---

[5]The absence of this mixing follows from the fact that the chiralities of the $(\bar{s}, b)$ pair of fields differ between these groups of operators. Chirality conservation of massless QCD prevents mixing of operators of the same dimension but distinct quark chiralities, even for nonvanishing quark masses. For the same reason, $Q^c_{5,6}$ do not mix into Q_{9V}.

scheme dependence of $C_{7\gamma}$ and C_{8g} already at the leading order. The scheme-dependence ultimately cancels out in observables. It is convenient and customary to define effective dipole coefficients [24, 25]

$$C_{7\gamma}^{\text{eff}}(\mu) = C_{7\gamma}(\mu) + \vec{y} \cdot \vec{C}_{Ap}, \tag{2.18}$$

$$C_{8g}^{\text{eff}}(\mu) = C_{8g}(\mu) + \vec{z} \cdot \vec{C}_{Ap}, \tag{2.19}$$

in such a fashion that the leading-order expression for $\mathcal{B}(B \to X_s \gamma)$ is proportional to $|C_{7\gamma}^{\text{eff}}|^2$ (or $|C_{7\gamma}^{\text{eff}}|^2 + |C_{7\gamma}'^{\text{eff}}|^2$, in the presence of primed operators). This ensures that $C_{7\gamma}^{\text{eff}}$ and $C_{8\gamma}^{\text{eff}}$ are scheme-independent to leading order. In the CBSM scenario, with our choice of operator basis and renormalization, including in particular anticommuting γ_5, the vectors $\vec{y}$, $\vec{z}$ and $\vec{C}_{Ap}$ read

$$\vec{y} = \left(0, 0, 0, 0, \frac{2m_c}{m_b}, \frac{2m_c}{3m_b}, -\frac{1}{3}, -\frac{4}{9}, -\frac{20}{3}, -\frac{80}{3}\right), \tag{2.20}$$

$$\vec{z} = \left(0, 0, 0, 0, 0, \frac{m_c}{m_b}, 1, -\frac{1}{6}, 20, -\frac{10}{3}\right), \tag{2.21}$$

$$\vec{C}_{Ap} = \left(C_1, C_2, C_3, C_4, C_5, C_6, C_3^p, C_4^p, C_5^p, C_6^p\right), \tag{2.22}$$

extending the SM case [18, 26–28].

As in the SM case, one can choose to go to a special scheme where the vectors $\vec{y}$ and $\vec{z}$ vanish by means of a finite renormalization of the four-quark operators

$$Q_i^A \to Q_i^A - y_i Q_{7\gamma} - z_i Q_{8g},$$

where Q_i^A is any of the four-quark operators whose Wilson coefficients appear in $\vec{C}_{Ap}$. In this special scheme, $C_{7\gamma}$ and C_{8g} are (to leading order) equal to $C_{7\gamma}^{\text{eff}}$ and C_{8g}^{eff}, respectively, by construction. The mixing among the four-quark operators is unaffected by the change of scheme, but the anomalous dimension elements involving the dipole operators change. The resulting leading-order anomalous dimension matrix in the special scheme is sometimes referred to as $\gamma^{(0),\text{eff}}$.

Let us now turn to case B. In this case, the mixing of the CBSM operators into the dipoles through $\vec{\gamma}_{B7}$ and $\vec{\gamma}_{B8}$ arises at one-loop order, but there is no mixing into the semileptonic coefficient C_{9V}. To restore the form (2.11) we should now rescale the electromagnetic and chromomagnetic dipoles as

$$Q_{7\gamma}(\mu) = \frac{4\pi}{\alpha_s(\mu)} \tilde{Q}_{7\gamma}(\mu), \qquad C_{7\gamma}(\mu) = \frac{\alpha_s(\mu)}{4\pi} \tilde{C}_{7\gamma}(\mu), \tag{2.23}$$

$$Q_{8g}(\mu) = \frac{4\pi}{\alpha_s(\mu)} \tilde{Q}_{8g}(\mu), \qquad C_{8g}(\mu) = \frac{\alpha_s(\mu)}{4\pi} \tilde{C}_{8g}(\mu). \tag{2.24}$$

This ensures that $\vec{\gamma}_{B7,8}$ begin at $\mathcal{O}(\alpha_s)$; at the same time it makes the blocks $\vec{\gamma}_{p7}$ and $\vec{\gamma}_{p8}$ vanish at $\mathcal{O}(\alpha_s)$. As was the situation for the semileptonic coefficients in case A, now the dipole coefficients are formally of order $\mathcal{O}(1/\alpha_s)$. Note that this makes the Standard Model contribution formally subleading. This is reflected in the fact that we will find below that

$\mathcal{B}(B \to X_s\gamma)$ poses extremely stringent constraints on $\vec{C}_B$, corresponding to BSM scales of tens of TeV. The leading-order dipole coefficients are now scheme-independent and are not complemented by finite leading-order contributions from the four-quark operators at leading order, i.e. there is no need to define effective dipole coefficients.

Since $\vec{C}_A$ and $\vec{C}_B$ do not mix under renormalization, and the mixing into the penguin and dipole coefficients is simply additive, there there is no problem patching together the solutions for both cases into an unambiguous and scheme-independent evolution operator. The part of the evolution matrix relevant for our phenomenology corresponds to the subset of coefficients $\vec{C}(\mu_b) = (\vec{C}^c(\mu_b), C_{7\gamma}^{\text{eff}}(\mu_b), C_{9V}(\mu_b))$, and with initial conditions $\vec{C}(\mu_0) = (\vec{C}^c(\mu_0), 0, 0)$ for $\mu_0 = M_W$ and $\mu_b = 4.2$ GeV this reads

$$
\begin{pmatrix} C_1^c(\mu_b) \\ C_2^c(\mu_b) \\ C_3^c(\mu_b) \\ C_4^c(\mu_b) \\ C_5^c(\mu_b) \\ C_6^c(\mu_b) \\ C_7^c(\mu_b) \\ C_8^c(\mu_b) \\ C_9^c(\mu_b) \\ C_{10}^c(\mu_b) \\ C_{7\gamma}^{\text{eff}}(\mu_b) \\ C_{9V}(\mu_b) \end{pmatrix} =
\begin{pmatrix}
1.1 & -0.27 & 0 & 0 & 0 & 0 & 0 & 0 & 0 & 0 \\
-0.27 & 1.1 & 0 & 0 & 0 & 0 & 0 & 0 & 0 & 0 \\
0 & 0 & 0.92 & 0 & 0 & 0 & 0 & 0 & 0 & 0 \\
0 & 0 & 0.33 & 1.9 & 0 & 0 & 0 & 0 & 0 & 0 \\
0 & 0 & 0 & 0 & 1.9 & 0.33 & 0 & 0 & 0 & 0 \\
0 & 0 & 0 & 0 & 0 & 0.92 & 0 & 0 & 0 & 0 \\
0 & 0 & 0 & 0 & 0 & 0 & 1.0 & 0.05 & 2.70 & 1.70 \\
0 & 0 & 0 & 0 & 0 & 0 & 0.37 & 2.0 & 2.30 & -0.55 \\
0 & 0 & 0 & 0 & 0 & 0 & 0.07 & 0.07 & 1.80 & 0.04 \\
0 & 0 & 0 & 0 & 0 & 0 & 0.01 & -0.02 & -0.29 & 0.82 \\
0.02 & -0.19 & -0.015 & -0.13 & 0.56 & 0.17 & -1.0 & -0.47 & 4.00 & 0.70 \\
8.50 & 2.10 & -4.30 & -2.00 & 0 & 0 & 0 & 0 & 0 & 0
\end{pmatrix}
\begin{pmatrix} C_1^c(M_W) \\ C_2^c(M_W) \\ C_3^c(M_W) \\ C_4^c(M_W) \\ C_5^c(M_W) \\ C_6^c(M_W) \\ C_7^c(M_W) \\ C_8^c(M_W) \\ C_9^c(M_W) \\ C_{10}^c(M_W) \end{pmatrix}.
$$

(2.25)

2.2.1 Remarks on computed and uncomputed ADM elements

As part of our earlier work [1], we made the first calculation of the mixing of the BSM operators $Q_{3,4}^c$ into the operators P_{3-6}, $Q_{7\gamma}$, and Q_{9V}. The mixing into the photon penguin $Q_{7\gamma}$ is the most technically challenging, arising from two-loop diagrams. We did not compute the two-loop mixing of $Q_{3,4}^c$ into the gluon penguin Q_{8g}, and neglect this mixing in our numerical results in both the previous work and this article – the corresponding result for the mixing of the SM operators $Q_{1,2}^c$ is known to produce only a very small effect on the contribution of $C_2(M_W)$ to $C_{7\gamma}^{\text{eff}}(\mu_b)$, and we expect a similarly small effect from the results we neglect. Further details can be found in the Appendix of [1].

3 Observables

In this section we collect a set of observables that are very sensitive to $(\bar{c}b)(\bar{s}c)$ operators and allow us thus to constrain the possible size of new $b \to c\bar{c}s$ contributions: the dominant weak annihilation contribution to the B_s lifetime, $\tau(B_s)$, is given by a $(\bar{c}b)(\bar{s}c)$ transition, which is also the leading term to the mixing induced decay rate difference of neutral B_s mesons, $\Delta\Gamma_s$. Taking a $(\bar{c}b)(\bar{s}c)$ operator and closing the charm quarks to a loop we get large penguin contributions, that sizeably affect $b \to s\gamma$ and $b \to s\ell\ell$ decays. Finally the gold-plated mode for CP-violation, $B_d \to J/\psi K_S$ is triggered by a tree-level $b \to c\bar{c}s$

decay. Below we determine the dependence of all these observables on the new four quark operators.

3.1 Lifetime ratio $\tau(B_s)/\tau(B_d)$

The total decay width of the B_s meson can be expressed as

$$\Gamma_s \equiv \frac{1}{\tau(B_s)} = \frac{1}{2M_{B_s}} \langle B_s \mid \mathcal{T} \mid B_s \rangle , \tag{3.1}$$

with the transition operator

$$\mathcal{T} = \text{Im} \left[i \int d^4 x T[\mathcal{H}_{\text{eff}}(x)\mathcal{H}_{\text{eff}}(0)] \right] . \tag{3.2}$$

According to the Heavy Quark Expansion (HQE) (see [29] for a review and early references) the transition operator can be expanded in inverse powers of the heavy b quark mass – each term in the expansion contains perturbative Wilson coefficients and non-perturbative matrix elements of $\Delta B = 0$ operators. We will investigate the precisely measured lifetime ratio

$$\frac{\tau(B_s)}{\tau(B_d)} = 1 + \frac{\Gamma_d - \Gamma_s}{\Gamma_s} \approx 1 + \frac{\Gamma_d^{\text{SM}} - \Gamma_s^{\text{SM}}}{\Gamma_s^{\text{SM}}} - \frac{\Gamma_s^{\text{BSM}}}{\Gamma_s} = \frac{\tau(B_s)^{\text{SM}}}{\tau(B_d)^{\text{SM}}} - \Gamma_s^{\text{BSM}}\tau(B_s)^{\text{exp}} . \tag{3.3}$$

The SM value of $\tau(B_s)/\tau(B_d)$ will be taken from [30], which uses perturbative input from [31, 32]. The leading contribution to this lifetime ratio is given by the third order in the HQE (see e.g. [29]) and the dominant contribution at this order to the B_s decay rate is given by $\Delta B = 1$ $b \to c\bar{c}s$ transitions. These transitions are CKM suppressed for the B_d meson. Thus we assumed in (3.3) that the BSM effects due to the new $b \to c\bar{c}s$ operators contribute only to Γ_s^{BSM} and the B_d lifetime agrees with the SM expectation. The leading (i.e. LO-QCD and dimension six in the HQE) new $b \to c\bar{c}s$ contributions are given by

$$\Gamma_s^{\text{BSM}} = \frac{8G_F^2}{M_{B_s}} |\lambda_c|^2 \sum_{i=1}^{20} \sum_{j=1}^{20} C_i^c (C_j^c)^* \langle B_s \mid \text{Im} \left\{ i \int d^4 x T \left[Q_i^c(x) Q_j^{c\dagger}(0) \right] \right\} \mid B_s \rangle - \Gamma_s^{\text{SM}}$$

$$= \frac{G_F^2 m_b^2 M_{B_s} f_{B_s}^2}{4\pi} N_c \sqrt{1-z} |\lambda_c|^2 \left[\sum_{i=1}^{20} \sum_{j=1}^{20} C_i^c (C_j^c)^* \Gamma(i,j) - \sum_{i=1}^{2} \sum_{j=1}^{2} C_i^{c,\text{SM}} (C_j^{c,\text{SM}})^* \Gamma(i,j) \right] . \tag{3.4}$$

The ratio of charm and bottom quark mass is denoted by $z = 4m_c^2/m_b^2$. To avoid a double counting of the SM contribution due to Q_1^c and Q_2^c, we subtract explicitly the SM contributions proportional to $C_i^{c,\text{SM}}(C_j^{c,\text{SM}})^*$. The terms $\Gamma(i,j)$ are symmetric ($\Gamma(i,j) = \Gamma(j,i)$) and they can be further split up into contributions of eight different $\Delta B = 0$ four-quark operators.

$$\begin{aligned}
Q_{XY} &= \left(\bar{b}\gamma_\mu P_X s\right) \left(\bar{s}\gamma^\mu P_Y b\right) , & Q_{XY}^S &= \left(\bar{b}P_X s\right) \left(\bar{s}P_Y b\right) , \\
\tilde{Q}_{XY} &= \left(\bar{b}^i\gamma_\mu P_X s^j\right) \left(\bar{s}^j\gamma^\mu P_Y b^i\right) , & \tilde{Q}_{XY}^S &= \left(\bar{b}^i P_X s^j\right) \left(\bar{s}^j P_Y b^i\right) ,
\end{aligned} \tag{3.5}$$

with $XY = LL, LR$. The matrix elements of these operators are parameterised as

$$\frac{1}{2M_{B_s}}\langle B_s|\overset{(\sim)}{Q}_{LL}, \overset{(\sim)}{Q}_{LR}|B_s\rangle = \frac{1}{8}\overset{(\sim)}{B}_{1,3}(\mu)f^2_{B_s}M_{B_s}\,,$$

$$\frac{1}{2M_{B_s}}\langle B_s|\overset{(\sim)}{Q}^S_{LR}, \overset{(\sim)}{Q}^S_{LL}|B_s\rangle = \frac{1}{8}\frac{M^2_{B_s}}{[\bar{m}_b(\bar{m}_b) + \bar{m}_s(\bar{m}_b)]^2}\overset{(\sim)}{B}_{2,4}(\mu)f^2_{B_s}M_{B_s}\,,$$

(3.6)

with the decay constant f_{B_s}. The bag parameters $\overset{(\sim)}{B}_{1,2}$ have been determined in [30], while for the remaining bag parameters we will use vacuum insertion approximation:

$$B_{3,4} = -1\,, \qquad \widetilde{B}_{3,4} = -\frac{1}{N_c}\,.$$

(3.7)

For the individual contributions we get (where we define

$$\overset{(\sim)'}{B}_{2,4} = \frac{M^2_{B_s}}{[\bar{m}_b(\bar{m}_b) + \bar{m}_s(\bar{m}_b)]^2}\overset{(\sim)}{B}_{2,4}$$

(3.8)

for the sake of brevity)

$$\Gamma(1,1) = \frac{1}{12}\left[2(z+2)B'_2 + (z-4)B_1\right]\,, \qquad \Gamma(1,3) = \frac{1}{8}zB_1\,, \qquad \Gamma(1,5) = -\frac{1}{2}\sqrt{z}B'_2\,,$$

$$\Gamma(1,9) = \frac{1}{2}\sqrt{z}(4B'_2 - B_1)\,, \qquad\qquad \Gamma(1,11) = -\frac{1}{4}zB_3\,, \quad \Gamma(1,7) = \frac{1}{8}\sqrt{z}B_1\,,$$

$$\Gamma(1,13) = -\frac{1}{24}\left[2(z+2)B'_4 + (z-4)B_3\right]\,, \quad \Gamma(1,15) = \frac{1}{2}\sqrt{z}B'_4\,,$$

(3.9)

$$\Gamma(1,17) = \frac{1}{8}\sqrt{z}\left[B_3 - 2B'_4\right]\,, \qquad\qquad \Gamma(1,19) = -\frac{1}{2}\sqrt{z}\left[2B'_4 + B_3\right]\,.$$

$$\Gamma(3,3) = \frac{1}{4}\Gamma(1,1)\,, \qquad \Gamma(3,7) = \frac{1}{16}\sqrt{z}\left(2B'_2 - B_1\right)\,, \quad \Gamma(3,5) = \frac{1}{2}\Gamma(1,5)\,,$$

$$\Gamma(3,13) = -\frac{1}{16}zB_3\,, \qquad \Gamma(3,9) = \frac{1}{4}\sqrt{z}\left(B_1 + 2B'_2\right)\,, \quad \Gamma(3,15) = \frac{1}{2}\Gamma(1,15)\,, \quad (3.10)$$

$$\Gamma(3,17) = -\frac{1}{16}\sqrt{z}B_3\,, \quad \Gamma(3,19) = \frac{1}{4}\sqrt{z}\left(B_3 - 4B'_4\right)\,.$$

$$\Gamma(5,5) = (2-z)B'_2\,, \quad \Gamma(5,7) = -\frac{1}{4}zB'_2\,, \qquad \Gamma(5,9) = 12\Gamma(5,7)\,,$$

$$\Gamma(5,15) = -zB'_4\,, \qquad \Gamma(5,17) = \frac{1}{4}(2-z)B'_4\,, \quad \Gamma(5,19) = 12\Gamma(5,17)\,.$$

(3.11)

$$\Gamma(7,7) = -\frac{1}{48}\left[(z+2)B_1 + 2(z-4)B'_2\right]\,, \quad \Gamma(7,17) = \frac{1}{4}\Gamma(1,11)\,,$$

$$\Gamma(7,9) = \frac{1}{12}\left[(z+2)B_1 + 2(8-5z)B'_2\right]\,, \quad \Gamma(7,19) = \frac{1}{4}z\left(B_3 - 4B'_4\right)\,.$$

(3.12)

$$\Gamma(9,9) = -\frac{1}{3}\left[(z+2)B_1 + 2(13z-28)B'_2\right]\,, \quad \Gamma(9,19) = -z\left(8B'_4 + B_3\right)\,.$$

(3.13)

All remaining terms can be extracted from those given via the following rules:

$$
\Gamma(i,j) = \begin{cases} \frac{1}{N_c}\Gamma(i-1,j-1)\big|_{B_i^{(\prime)}\to\tilde{B}_i^{(\prime)}} & \text{for } i,j \text{ even}, \\ \frac{1}{N_c}\Gamma(i-1,j) & \text{for } i \text{ even}, j \text{ odd}, \\ \frac{1}{N_c}\Gamma(i,j-1) & \text{for } i \text{ odd}, j \text{ even}, \\ \Gamma(i-10,j-10) & \text{for } i,j > 10, \\ \Gamma(j-10,i+10) & \text{for } i < 10, j > 10, i > j - 10, \\ \Gamma(j,i) & \text{for } i > j. \end{cases} \tag{3.14}
$$

The interested reader can download a `Mathematica` program containing the full algebraic expressions from the arXiv version of this article .

3.2 B_s mixing observables $\Delta\Gamma_s$ and a_{sl}^s

The decay rate difference of neutral B_s mesons, $\Delta\Gamma_s$, and the flavour specific CP asymmetry in B_s decays, a_{sl}^s, are sensitive to new $b \to c\bar{c}s$ effects. Using the conventions of [33] we get

$$
\Delta\Gamma_s = 2|\Gamma_{12}^s|\cos\phi_{12}^s\,, \qquad a_{sl}^s = \left|\frac{\Gamma_{12}^s}{M_{12}^s}\right|\sin\phi_{12}^s\,, \tag{3.15}
$$

where Γ_{12}^s denotes the absorptive part of the mixing diagrams and M_{12}^s the dispersive part. The relative phase of these contributions is defined as

$$
\phi_{12}^s := \arg\left(-\frac{M_{12}^s}{\Gamma_{12}^s}\right). \tag{3.16}
$$

Similar to the case of the total decay rate the off diagonal matrix element of the absorptive part of the $B_s - \bar{B}_s$ mixing matrix, Γ_{12}^s can be expressed in terms of double insertion of the effective Hamiltonian

$$
\Gamma_{12}^s = \frac{1}{2M_{B_s}}\langle B_s|\mathcal{T}|\bar{B}_s\rangle\,, \qquad \text{with} \qquad \mathcal{T} = \text{Im}\left[i\int d^4x\, T[\mathcal{H}_{\text{eff}}(x)\mathcal{H}_{\text{eff}}(0)]\right]. \tag{3.17}
$$

This matrix element can be split up into a SM contribution and a BSM contribution due to the new $b \to c\bar{c}s$ transitions

$$
\Gamma_{12}^s = \Gamma_{12}^{\text{SM}} + \Gamma_{12}^{c\bar{c}}\,. \tag{3.18}
$$

The numerical value of the SM part is based on [34–37], the BSM part is further decomposed as

$$
\begin{aligned}
\Gamma_{12}^{c\bar{c}} &= \frac{4G_F^2\lambda_c^2}{M_{B_s}}\sum_{i=1}^{20}\sum_{j=1}^{20}C_i^c C_j^c\langle B_s|\text{Im}\left\{i\int d^4x\, T[Q_i^c(x)Q_j^c(0)]\right\}|\bar{B}_s\rangle \\
&= \frac{G_F^2\lambda_c^2 m_b^2 M_{B_s}f_{B_s}^2}{12\pi}\sqrt{1-z}\left[8G(z)B + F(z)\tilde{B}_S'\right] + \mathcal{O}\left(\frac{\Lambda_{QCD}}{m_b}\right) + \mathcal{O}(\alpha_s)\,.
\end{aligned} \tag{3.19}
$$

The arising four quark operators can be parametrised as

$$
\langle Q\rangle = \frac{8}{3}M_{B_s}^2 f_{B_s}^2 B\,, \qquad \langle\tilde{Q}_S\rangle = \frac{1}{3}M_{B_s}^2 f_{B_s}^2 \tilde{B}_S'\,, \tag{3.20}
$$

with

$$\tilde{B}'_S = \frac{M^2_{B_s}}{(\bar{m}_b(\bar{m}_b) + \bar{m}_s(\bar{m}_b))^2}\tilde{B}_S \,, \tag{3.21}$$

which matches the definition in [33]; these bag parameters have been recently determined in [38–40]. The coefficient functions read

$$
\begin{aligned}
F(z) = {}& \left(1 + \frac{z}{2}\right)\left[\frac{C_1^{c,2} - (C_1^{c,\text{SM}})^2}{2} + \frac{C_1^c C_2^c - C_1^{c,\text{SM}}C_2^{c,\text{SM}}}{3} - \frac{C_2^{c,2} - (C_2^{c,\text{SM}})^2}{6} + \frac{C_3^{c,2}}{8} + \frac{C_3^c C_4^c}{12} - \frac{C_4^{c,2}}{24}\right] \\
& - \left(1 - \frac{z}{2}\right)\left[18\,C_5^c C_9^c + 6(C_5^c C_{10}^c + C_6^c C_9^c - C_6^c C_{10}^c) + \frac{3}{2}C_5^c C_7^c + \frac{C_5^c C_8^c + C_6^c C_7^c - C_6^c C_8^c}{2}\right] \\
& + \sqrt{z}\left[6C_1^c C_9^c + 2C_1^c C_{10}^c + 2C_2^c C_9^c - 2C_2^c C_{10}^c - \frac{3}{2}(C_1^c C_5^c - C_3^c C_9^c) - \frac{3}{4}C_3^c C_5^c + \frac{3}{8}C_3^c C_7^c\right. \\
& \left. \quad - \frac{C_1^c C_6^c + C_2^c C_5^c - C_2^c C_6^c - C_3^c C_{10}^c - C_4^c C_9^c + C_4^c C_{10}^c}{2} - \frac{C_3^c C_6^c + C_4^c C_5^c - C_4^c C_6^c}{4}\right. \\
& \left. \quad + \frac{C_3^c C_8^c + C_4^c C_7^c - C_4^c C_8^c}{8}\right] + z\left[15C_9^{c,2} + 10C_9^c C_{10}^c - 5C_{10}^{c,2} + \frac{3}{2}C_7^c C_9^c + \frac{3}{2}C_5^{c,2} + C_5^c C_6^c\right. \\
& \left. \quad + \frac{C_7^c C_{10}^c + C_8^c C_9^c - C_8^c C_{10}^c}{2} - \frac{C_6^{c,2}}{2} + \frac{C_7^c C_8^c}{8} + \frac{3C_7^{c,2} - C_8^{c,2}}{16}\right] \\
& + \left(C_i^c C_j^c \to C_i^{c'} C_j^{c'} \,, C_{1,2}^{c,\text{SM}} \to 0\right) \tag{3.22}
\end{aligned}
$$

and

$$
\begin{aligned}
G(z) = {}& -\left(1 - \frac{z}{2}\right)\left[9C_5^c C_9^c + 3(C_5^c C_{10}^c + C_6^c C_9^c) + \frac{3C_5^c C_7^c + C_5^c C_8^c + C_6^c C_7^c}{4}\right] \\
& - (1 - z)\left[\frac{C_1^{c,2} - (C_1^{c,\text{SM}})^2}{4} + \frac{C_1^c C_2^c - C_1^{c,\text{SM}}C_2^{c,\text{SM}}}{6} + \frac{C_3^{c,2}}{16} + \frac{C_3^c C_4^c}{24}\right] \\
& - \left(1 - \frac{z}{4}\right)\left[\frac{C_2^{c,2} - (C_2^{c,\text{SM}})^2}{6} + \frac{C_4^{c,2}}{24}\right] + z\left[6C_9^{c,2} + 4C_9^c C_{10}^c + \frac{3}{2}C_7^c C_9^c - \frac{C_8^{c,2}}{32}\right. \\
& \left. \quad + \frac{C_7^c C_{10}^c + C_8^c C_9^c - C_{10}^{c,2}}{2} + \frac{C_8^c C_{10}^c}{4} + \frac{3}{4}C_5^{c,2} + \frac{C_5^c C_6^c}{2}\right. \\
& \left. \quad + \frac{3C_1^c C_3^c + C_1^c C_4^c + C_2^c C_3^c + C_2^c C_4^c}{8}\right] + \sqrt{z}\left[\frac{3}{2}(C_1^c C_9^c + C_3^c C_9^c) - \frac{3}{4}C_1^c C_5^c\right. \\
& \left. \quad + \frac{C_1^c C_{10}^c + C_2^c C_9^c - C_2^c C_{10}^c + C_3^c C_{10}^c + C_4^c C_9^c}{2} + \frac{3}{8}(C_1^c C_7^c - C_3^c C_5^c)\right. \\
& \left. \quad - \frac{C_1^c C_6^c + C_2^c C_5^c - C_4^c C_{10}^c}{4} + \frac{C_1^c C_8^c + C_2^c C_7^c + C_2^c C_8^c - C_3^c C_6^c - C_4^c C_5^c}{8} - \frac{C_4^c C_8^c}{16}\right] \\
& + \left(C_i^c C_j^c \to C_i^{c'} C_j^{c'} \,, C_{1,2}^{c,\text{SM}} \to 0\right) \,. \tag{3.23}
\end{aligned}
$$

The interested reader can download a `Mathematica` program containing the full algebraic expressions from the arXiv version of this article.

At this point we would like to mention that neglecting the CKM structure λ_u (as advocated in Section 2) might result in misleading conclusions for the semileptonic CP

asymmetry – depending on the experimental precision of the corresponding measurement. The mixing observables can also be determined via the following relations

$$\frac{\Delta\Gamma_s}{\Delta M_s} = -\mathcal{R}\left(\frac{\Gamma_{12}^s}{M_{12}^s}\right), \qquad a_{sl}^s = \mathcal{I}\left(\frac{\Gamma_{12}^s}{M_{12}^s}\right).$$ (3.24)

Using the notation in [33] and CKM unitarity ($\lambda_u + \lambda_c + \lambda_t = 0$) we can further simplify

$$\begin{aligned}
-\frac{\Gamma_{12}^s}{M_{12}^s} &= \frac{\lambda_c^2\Gamma_{12}^{s,cc} + 2\lambda_c\lambda_u\Gamma_{12}^{s,uc} + \lambda_u^2\Gamma_{12}^{s,uu}}{\lambda_t^2\tilde{M}_{12}^s} \\
&= \frac{\Gamma_{12}^{s,cc}}{\tilde{M}_{12}^s} + 2\frac{\lambda_u}{\lambda_t}\frac{\Gamma_{12}^{s,cc} - \Gamma_{12}^{s,uc}}{\tilde{M}_{12}^s} + \left(\frac{\lambda_u}{\lambda_t}\right)^2\frac{\Gamma_{12}^{s,cc} - 2\Gamma_{12}^{s,uc} + \Gamma_{12}^{s,uu}}{\tilde{M}_{12}^s} \\
&= -10^{-4}\left[c + a\frac{\lambda_u}{\lambda_t} + b\left(\frac{\lambda_u}{\lambda_t}\right)^2\right].
\end{aligned}$$ (3.25)

The real coefficients show a clear hierarchy $c \gg a \gg b$ and the small ratio of CKM elements λ_u/λ_t has an imaginary part. Thus in the SM the value of $\Delta\Gamma_s/\Delta M_s$ is well approximated by the term proportional to c, while a_{sl}^s is well approximated by the term proportional to a. We see from (3.25) that the approximation $\lambda_u = 0$ yields a vanishing semileptonic CP asymmetry. Since the current experimental uncertainty of a_{sl}^s is about a factor of 130 larger than the SM central value of this quantity, neglecting λ_u gives reasonable results. Moreover complex Wilson coefficients can have large effects in the semileptonic CP asymmetry by creating an imaginary part in the coefficient c, that does not suffer from the CKM suppression due to the factor λ_u/λ_t.

3.3 The radiative decay $B \to X_s\gamma$

It is well known that weak radiative B meson decays are sensitive to BSM physics. The Standard-Model prediction of the branching ratio for $\mathcal{B}(\bar{B} \to X_s\gamma)^{\text{SM}} = (3.36\pm0.23)\times10^{-4}$ [41] is in good agreement with the current experimental average of $\mathcal{B}(\bar{B} \to X_s\gamma)^{\text{exp}} = (3.32 \pm 0.15) \times 10^{-4}$ [42]. In accordance with Heavy Quark Effective Theory (HQET) we may express the inclusive decay rate for a B meson into a charmless hadron and a photon as

$$\Gamma(\bar{B} \to X_s\gamma) \simeq \Gamma(b \to X_s^{\text{parton}}\gamma) + \delta^{\text{np}},$$ (3.26)

Here the non-perturbative term δ^{np}, for $E_\gamma > E_0$ with the lower cut off of the photon energy $E_0 = 1.6\,\text{GeV}$, is estimated to be at the $(3 \pm 5)\%$ level [43, 44]. Following the approach of [45, 46] the branching ratio $\mathcal{B}(\bar{B} \to X_s\gamma)$ can be expressed as

$$\mathcal{B}(\bar{B} \to X_s\gamma)_{E_0>E_\gamma} = \mathcal{B}(\bar{B} \to X_ce\bar{\nu})^{\text{exp}}\left|\frac{V_{ts}^*V_{tb}}{V_{cb}}\right|^2\frac{6\alpha_{em}}{\pi C}\left[P(E_0) + N(E_0)\right],$$ (3.27)

where $P(E_0)$ and $N(E_0)$ denote, respectively, the leading-power perturbative contribution and non-perturbative corrections, and C is defined as

$$C = \left|\frac{V_{ub}}{V_{cb}}\right|^2\frac{\Gamma(\bar{B} \to X_ce\bar{\nu})}{\Gamma(\bar{B} \to X_ue\bar{\nu})}.$$ (3.28)
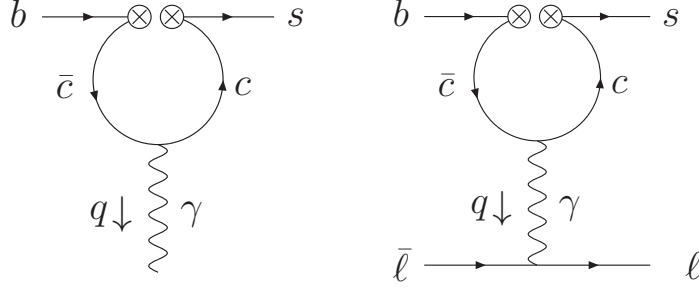
Figure 1: Leading CSBM contribution to radiative decay (left) and rare $b \to s\ell\ell$ decays (right).

We neglect BSM corrections to the non-perturbative part and split the perturbative term $P(E_0)$ into an SM part and a BSM part,

$$P(E_0) = P^{\text{SM}}(E_0) + P^{\text{BSM}}(E_0). \tag{3.29}$$

We similarly split the branching ratio,

$$\mathcal{B}(\bar{B} \to X_s\gamma) = \mathcal{B}(\bar{B} \to X_s\gamma)_{\text{SM}} + \Delta\mathcal{B}_{\text{BSM}}. \tag{3.30}$$

To zeroth order in α_s and neglecting the strange quark mass, we have

$$P^{\text{BSM}}(E_0) = 2C_{7\gamma}^{\text{eff,SM}}\text{Re}(\bar{C}_{7\gamma}^{\text{eff}}) + |\bar{C}_{7\gamma}^{\text{eff}}|^2 + |\bar{C}_{7\gamma}'^{\text{eff}}|^2, \tag{3.31}$$

which follows from substituting $C_{7\gamma}^{\text{eff}} \to C_{7\gamma}^{\text{eff,SM}} + \bar{C}_{7\gamma}^{\text{eff}}$ in the SM expression. The barred coefficients are defined as

$$\bar{C}_{7\gamma}^{\text{eff}}(q^2,\mu) = C_{7\gamma}^{\text{eff,BSM}}(\mu) + \frac{m_c}{m_b}\left[\left(4\Delta C_{9,10}^c(\mu) - \Delta C_{7,8}^c(\mu)\right)y(q^2,\mu) - \frac{\Delta C_{7,8}^c(\mu)}{6}\right], \tag{3.32}$$

$$\bar{C}_{7\gamma}'^{\text{eff}}(q^2,\mu) = C_{7\gamma}'^{\text{eff,BSM}}(\mu) + \frac{m_c}{m_b}\left[\left(4\Delta C_{9,10}^{c'}(\mu) - \Delta C_{7,8}^{c'}(\mu)\right)y(q^2,\mu) - \frac{\Delta C_{7,8}^{c'}(\mu)}{6}\right], \tag{3.33}$$

where $\Delta C_{x,y}^c(\mu) = 3\Delta C_x^c(\mu) + \Delta C_y^c(\mu)$ and

$$y(q^2,m_c,\mu) = -\frac{1}{3}\left[\ln\frac{m_c^2}{\mu^2} - \frac{3}{2} + 2a(z)\right], \tag{3.34}$$

with $a(z) = \sqrt{|z-1|}\arctan\frac{1}{\sqrt{z-1}}$ and $z = 4m_c^2/q^2$. That is to say, in addition to the BSM corrections to the Wilson coefficients $C_{7\gamma}^{(\prime)\,\text{eff}}$, which arise from large logarithms in the charm loop and are included through leading-order RG evolution as described in Section 2.2, we also include the remainder of the charm loop (see left diagram in Figure 1). For the SM contribution and BSM contributions to $C_{1\ldots4}^{c\,(\prime)}$, this is a constant of UV origin and is already included in $C_7^{(\prime)\,\text{eff,BSM}}$. In contradistinction, in the presence of nonzero CBSM coefficients $C_{7\ldots10}^{c\,(\prime)}$ a q^2-dependent contribution appears, as is evident from the expressions. This comes

together with a large logarithm at $\mathcal{O}(\alpha_s^0)$, which causes a 1-loop mixing into $C_{7\gamma}^{\text{eff}\,(\prime)}$, making the BSM contribution formally $\mathcal{O}(1/\alpha_s)$ and leading over the SM, as already mentioned in Section 2.2. In consequence, the finite contribution is formally subleading, as well as scheme-dependent.[6] However, the q^2 dependence itself is a leading effect, and in any case is a qualitatively new feature, which is why we present it here. For the coefficients $C_{5,6}^{c\,(\prime)}$, only a constant term is present and the mixing arises at two-loop order, mirroring the situation of the SM.

With expressions (3.29), (3.30) and (3.31) we determine the shift to the SM branching ratio in terms of the charmed four fermion coefficients and in Section 4 find this leads, in many cases, to stringent constraints on their BSM parts $\Delta C_i^{c(\prime)}$. For the numerics in this work we use $m_c = m_{c,\text{pole}}$ and work in the $q^2 \to 0$ limit.

3.4 Rare $b \to s\ell\ell$ decays

The rare decays $B \to K^{(*)}\ell^+\ell^-$ are also calculable to leading order in the heavy-quark expansion [47]. Through zeroth order in α_s, they receive CBSM contributions both through $\bar{C}_{7\gamma}^{(\prime)\,\text{eff}}(q^2,\mu)$ defined in the previous subsection and through further coefficients $C_9^{(\prime)\text{eff}}(q^2,\mu)$ (see Figure 1 (right) for the contributing Feynman diagram). The CBSM contributions to the latter have the form

$$C_9^{\text{eff,BSM}}(q^2,\mu) = C_{9V}^{\text{BSM}}(\mu) + \left(\Delta C_{1,2}^c(\mu) - \frac{\Delta C_{3,4}^c(\mu)}{2}\right) h(q^2,\mu) - \frac{2}{9}\Delta C_{3,4}^c(\mu)\,, \quad (3.35)$$

$$C_9^{\prime\text{eff,BSM}}(q^2,\mu) = C_{9V}^{\prime\text{BSM}}(\mu) + \left(\Delta C_{1,2}^{c\prime}(\mu) - \frac{\Delta C_{3,4}^{c\prime}(\mu)}{2}\right) h(q^2,\mu) - \frac{2}{9}\Delta C_{3,4}^{c\prime}(\mu)\,, \quad (3.36)$$

where

$$h(q^2,m_c,\mu) = -\frac{4}{9}\left[\ln\frac{m_c^2}{\mu^2} - \frac{2}{3} + (2+z)a(z) - z\right].\quad (3.37)$$

This q^2-dependent contribution to the rare $b \to s\ell\ell$ decays was a novel feature in our previous work [1], where we showed that, if the new physics scale is low enough, it can be potentially observable. This contrasts with statements elsewhere in literature where such a q^2 dependence was claimed to be an unambiguous criterion that the anomalies in the $B \to K^*\ell^+\ell^-$ angular distribution are of a hadronic origin. In the present work, we stick to new physics scales above the weak scale (as in the "high-scale scenario" of [1]). In this situation, C_{9V} is formally $\mathcal{O}(1/\alpha_s)$ already in the SM, although about half the numerical value originates from the $\mathcal{O}(1)$, formally subleading, Wt loop. Our q^2-dependent contributions are formally at the same order but turn out to be a numerically small correction. The q^2-independent contribution to $C_{9V}^{(\prime)}$, however, can be dramatic. In particular, when ΔC_1^c or ΔC_3^c are nonvanishing, it is easy to generate an $\mathcal{O}(1)$ shift to C_{9V}, while satisfying other constraints, as already stressed in [1]. Similarly, $\Delta C_{1,3}^{c\prime}$ strongly mix into C_{9V}', which will allow us to set stringent constraints on these coefficients in Section 4 below.

---

[6]This scheme dependence will cancel against a corresponding scheme-dependence in the (uncomputed) NLO correction to $C_7^{\text{eff}\,(\prime)}$, which involves two-loop mixing as well as the UV contribution to $C_{7\gamma}^{(\prime)}$

The scheme dependence of these effective coefficients enters through the h and y functions – in general the constant terms will vary depending on the choice of scheme. In principle there is also a model-dependent contribution arising from the matching of the UV theory, which in this paper we choose to ignore to keep our results model-independent.

When we consider the phenomenology in Section 4, we directly use $C_9'^{\mathrm{eff,BSM}}(q^2, \mu)$ and $\bar{C}_{7\gamma}'^{\mathrm{eff}}(q^2, \mu)$ as "observables" and show the constraints they impose upon the coefficients $\Delta C_i^{c'}$. Again, for the numerics in this work we use $m_c = m_{c,\mathrm{pole}}$. We will take $q^2 = 0$ for $\bar{C}_{7\gamma}^{(\prime)}$, but will consider $C_9'^{\mathrm{eff,BSM}}$ at $q^2 = 5\,\mathrm{GeV}^2$. This is because the former is primarily constrained from polarisation observables in radiative decay and the low-q^2 end of the $B \to K^* \ell^+ \ell^-$ dilepton mass distribution, while $C_9'^{\mathrm{eff,BSM}}$, if present, will become important away from the endpoint. We also note that $C_9'^{\mathrm{eff}}$ and $C_7'^{\mathrm{eff}}$ are negligible in the SM.

3.5 The hadronic decay $B_d \to J/\psi K_S$

The $b \to c\bar{c}s$ operators listed in Section 2 trigger the neutral B meson decay $B_d \to J/\psi K_S$. As a peculiar feature, both B_d and $\bar{B}_d$ can decay into the $J/\psi K_S$ final state, giving rise to a time-dependent CP-asymmetry via mixing-decay interference. The amplitudes of these colour-suppressed tree-level decays read

$$\bar{\mathcal{A}}_{J/\psi K_S} = \langle J/\psi K_S | \mathcal{H}_{\mathrm{eff}} | \bar{B}_d \rangle = \frac{4\,G_F}{\sqrt{2}} \lambda_c \sum_i C_i^c \langle J/\psi K_S | Q_i | \bar{B}_d \rangle \,, \tag{3.38}$$

$$\mathcal{A}_{J/\psi K_S} = \langle J/\psi K_S | \mathcal{H}_{\mathrm{eff}} | B_d \rangle = -\frac{4\,G_F}{\sqrt{2}} \lambda_c^* \sum_i C_i^{c*} \langle J/\psi K_S | Q_i | \bar{B}_d \rangle \,, \tag{3.39}$$

where the hadronic matrix elements $\langle J/\psi K_S | Q_i | \bar{B}_d \rangle$ contain the (CP-even) strong rescattering phases and the minus sign arises from $\eta_{\mathrm{CP}}(J/\psi K_S) = -1$. Their determination is a non-perturbative problem which at present cannot be solved from first principles. We will develop a strategy to extract partial information on these matrix elements, jointly with information on the Wilson coefficients, from experiment in the following.

Let us express the branching ratio and time-dependent CP-asymmetry in terms of the Wilson coefficients and hadronic matrix elements. Defining

$$\langle Q_i^c \rangle = \langle J/\psi K_S | Q_i^c | \bar{B}_d \rangle, \qquad r_{i1} = \frac{\langle Q_i^c \rangle}{\langle Q_1^c \rangle} \in \mathbb{C} \,, \tag{3.40}$$

the branching ratio reads

$$\mathcal{B}(B_d \to J/\psi K_S) = \frac{\tau_{B_d} p_c G_F^2 \, |\lambda_c|^2}{M_{B_d}^2 \pi} \, |\langle Q_1^c \rangle|^2 \, |C_1^c + C_2^c r_{21} + C_3^c r_{31} + C_4^c r_{41}|^2 \,,$$

where $p_c = 1.683$ GeV [48] is the momentum of the final-state particles in the rest frame of the B_d meson.

In writing (3.41) we have omitted penguin contributions, which in what follows will be negligible compared to the uncertainties stemming from the hadronic matrix elements, due to their small Wilson coefficients.

For the time-dependent CP-asymmetry, we neglect the tiny decay rate difference $\Delta\Gamma_d$, such that it takes the form

$$A_{CP}(t) = \frac{\Gamma\left[\bar{B}_d(t) \to J/\psi K_S\right] - \Gamma\left[B_d(t) \to J/\psi K_S\right]}{\Gamma\left[\bar{B}_d(t) \to J/\psi K_S\right] + \Gamma\left[B_d(t) \to J/\psi K_S\right]}$$

$$= S_{J/\psi K_S}\sin(\Delta M_d t) - C_{J/\psi K_S}\cos(\Delta M_d t)\,, \tag{3.41}$$

where ΔM_d is the precisely measured mass difference in the B_d system. Defining also

$$\lambda_{J/\psi K_S} = \frac{q_B}{p_B}\frac{\bar{\mathcal{A}}_{J/\psi K_S}}{\mathcal{A}_{J/\psi K_S}} = -\frac{V_{tb}^* V_{td}}{V_{tb} V_{td}^*}\frac{\lambda_c}{\lambda_c^*}\frac{C_1^c + r_{21}C_2^c + r_{31}C_3^c + r_{41}C_4^c}{C_1^{c*} + r_{21}C_2^{c*} + r_{31}C_3^{c*} + r_{41}C_4^{c*}}\,, \tag{3.42}$$

the mixing-induced asymmetry $S_{J/\psi K_S}$ and the direct CP asymmetry $C_{J/\psi K_S}$ are expressed as

$$S_{J/\psi K_S} = \frac{2\,\mathrm{Im}\,\lambda_{J/\psi K_S}}{1 + |\lambda_{J/\psi K_S}|^2}, \qquad C_{J/\psi K_S} = \frac{1 - |\lambda_{J/\psi K_S}|^2}{1 + |\lambda_{J/\psi K_S}|^2}. \tag{3.43}$$

In writing (3.42), we have neglected CP violation in the Kaon system and, for the final expression, taken $q_B/p_B = \frac{V_{tb}^* V_{td}}{V_{tb} V_{td}^*} = e^{-2i\beta + \mathcal{O}(\lambda^4)}$, which amounts to omitting CP-violation in mixing ($\lambda \approx 0.22$ is the Wolfenstein parameter).

If the Wilson coefficients are real (recall their phase convention is fixed by (2.2)), the unknown hadronic matrix elements cancel out in (3.42) and, taking into account the tiny measured value of $C_{J/\psi K_S}$, one obtains $S_{J/\psi K_S} \approx \mathrm{Im}(\lambda_{J/\psi K_S}) \approx \sin(2\beta)$ to percent-level accuracy, as in the SM. Once the Wilson coefficients become complex, this is no longer true and the S- and C-parameters become theoretically very uncertain. However, together with the branching fraction, they still comprise three observables, allowing to jointly determine up to three parameters. Consider now a scenario where new physics only affects C_1^c or C_2^c. In this case, the only nonperturbative input to the three observables is $|\langle Q_1^c\rangle|$ and r_{21}, comprising three real parameters in total. Hence it is sufficient to have theoretical control over *one* of these parameters in order to obtain a constraint in the complex C_1^c (or C_2^c) plane, generally a band.

To proceed, let us use a Fierz-transformed basis

$$O_1^c = (\bar{s}_L^i \gamma_\mu b_L^i)(\bar{c}_L^j \gamma^\mu c_L^j)\,, \quad O_2^c = (\bar{s}_L^i \gamma_\mu b_L^j)(\bar{c}_L^j \gamma^\mu c_L^i)\,, \tag{3.44}$$

$$O_3^c = (\bar{s}_L^i \gamma_\mu b_L^i)(\bar{c}_R^j \gamma^\mu c_R^j)\,, \quad O_4^c = (\bar{s}_L^i \gamma_\mu b_L^j)(\bar{c}_R^j \gamma^\mu c_R^i)\,, \tag{3.45}$$

which relate to the operators defined in (2.3) via

$$Q_1^c = O_1^c\,, \quad Q_2^c = O_2^c\,, \quad Q_3^c = -\frac{1}{2}O_3^c\,, \quad Q_4^c = -\frac{1}{2}O_4^c\,. \tag{3.46}$$

The hadronic matrix element $\langle O_1^c\rangle = \langle Q_1^c\rangle$ factorizes naively in the limit of a large number of colours. More precisely,

$$\langle O_1^c\rangle = \langle J/\psi|\bar{c}_L^i \gamma^\mu|0\rangle\langle K_S|\bar{s}_L^i \gamma_\mu b_L^i|\bar{B}_d\rangle\left(1 + \mathcal{O}(1/N_c^2)\right) \tag{3.47}$$

$$= \frac{M_{B_d}}{2}p_c f_{J/\psi}F^{B\to K}(q^2 = M_{J/\psi}^2)\left(1 + \mathcal{O}(1/N_c^2)\right)\,, \tag{3.48}$$

resulting in an uncertainty of only $\mathcal{O}(10-20\%)$ from form factor uncertainty and (non-factorizable) corrections to the $N_c \to \infty$ limit. Taking $F^{B \to K}(M^2_{J/\psi}) = 0.68 \pm 0.06$ (see Section 4.1.6), one obtains

$$|\langle O^c_1 \rangle| = \left[1.23 \pm 0.11 + \mathcal{O}\left(\frac{1}{N^2_c}\right)\right] \text{GeV}^3 = (1.23 \pm 0.18)\,\text{GeV}^3, \qquad (3.49)$$

where in the last expression we have taken $1/N^2_c = 1/9$ and combined errors in quadrature. This provides the required theoretical constraint. The three observables can now be used to jointly constrain the complex Wilson coefficient and the complex matrix element ratio r_{21}. In a global fit, this amounts to determining r_{21} from data. This is the strategy which will be followed in our phenomenology below.

The fact that r_{21} can (in the limited scenarios described) be determined from data motivates us to review expectations for the other operator matrix elements. Let us write them as the sum of a naive-factorization result and a correction term,

$$\langle J/\psi K_S | O^c_i | \bar{B}_d \rangle = \frac{M_{B_d}}{2} p_c f_{J/\psi} F^{B \to K}(q^2 = M^2_{J/\psi}) \left[r_0 + \sum_{n=1}^{\infty} r_n \alpha^n_s + \mathcal{O}\left(\frac{\Lambda_{\text{QCD}}}{\alpha_s m_c}\right)\right], \qquad (3.50)$$

The constant r_0 amounts to the naive-factorization term, $r_0 = 1$ for O^c_1 and O^c_3 and $r_0 = 1/3$ for O^c_2 and O^c_4. QCD factorization in the heavy quark limit [49] implies that the coefficients r_n, $n \geq 1$, are perturbatively calculable but that there is also a power correction "suppressed" by only $\Lambda_{\text{QCD}}/(\alpha_s m_c)$. (See also [50, 51].) As this power correction remains, at present, incalculable, one does not expect predictivity, beyond the large-N_c argument already presented. From a large-N_c perspective, the corrections to naive factorization are $1/N^2_c$-suppressed for both O_1 and O_3, but are unsuppressed for O_2, O_4.

The importance of contributions that do not naively factorize (often called 'non-factorizable') for these two operators becomes clearest by rewriting

$$O^c_2 = \frac{1}{N_c} O^c_1 + 2T^c_1, \quad O^c_4 = \frac{1}{N_c} O^c_3 + 2T^c_3, \qquad (3.51)$$

where

$$T^c_1 = (\bar{s}^i_L T^a_{ij} \gamma_\mu b^j_L)(\bar{c}^k_L T^a_{kl} \gamma^\mu c^l_L), \quad T^c_3 = (\bar{s}^i_L T^a_{ij} \gamma_\mu b^j_L)(\bar{c}^k_R T^a_{kl} \gamma^\mu c^l_R). \qquad (3.52)$$

The matrix elements of the colour-octet operators $T^c_{1,3}$ vanish altogether in naive factorization, i.e. $r_0 = 0$ for them, and they appear with large coefficients in (3.51).

Therefore the naive-factorization values

$$r^{(\text{NF})}_{21} = \frac{1}{N_c}, \quad r^{(\text{NF})}_{41} = \frac{1}{N_c}. \qquad (3.53)$$

should be expected to receive large corrections, whereas $r_{31} = 1 + \mathcal{O}(1/N^2_C)$. The situation is further aggravated in the decay amplitude, which is proportional to the combination $C^c_1(\mu) + r_{21} C^c_2(\mu)$, the so-called colour-suppressed tree amplitude which entails a severe cancellation in the SM case.

Quantitative estimates of r_{21} beyond naive factorization have been obtained using QCD factorisation and/or light-cone sum rules, [50–52]. In these approaches, the amplitude is usually parameterized as

$$\mathcal{N}\langle O_1^c\rangle^{\text{NF}} a_2,$$

where $\mathcal{N}$ is a normalization and the scheme- and scale-independent combination a_2 is related to r_{12} as

$$a_2 = C_1^c(\mu) + r_{21}(\mu)C_2^c(\mu) + \mathcal{O}(\alpha_s^2). \tag{3.54}$$

For instance, the NLO QCD factorization results for a_2 in [51] give $r_{21}(m_b) = 0.41 - 0.04i$ or $r_{21}(m_b) = 0.28 - 0.051i$ for two different models of the J/ψ light-cone distribution amplitudes. Both numbers include an estimate of twist-three (Λ/m_b) power corrections but neglect the $\mathcal{O}(\Lambda/(\alpha_s m_c))$ corrections, which as we have said provide an (additional) uncertainty. By comparison, the LCSR computation in [52] finds values closer to NF. These numbers can be contrasted to the 'experimental' value $r_{21}(m_b) \sim 0.46$. It is important, however, to note that this assumes the absence of NP in the Wilson coefficients C_1^c, C_2^c (and in addition vanishing relative phase between the hadronic matrix elements.) As we will see later, this assumption is not implied by current experimental data when NP in $b \to c\bar{c}s$ transitions is allowed.

4 Phenomenology

4.1 Numerical Inputs

In this section, we describe all the numerical inputs that are used in our work, along with the experimental results and their corresponding uncertainties. We break these down into a set of fundamental inputs that are common to all our different observables, and then some specific input parameters for the individual observables. Recall that quark masses are in the $\overline{\text{MS}}$ scheme unless indicated otherwise.

4.1.1 Common inputs

We show in Table 2 input parameters that are common to all our theoretical predictions. These inputs are taken from the Particle Data Group (PDG) [48] and the CKMfitter group [22] (similar results for the CKM elements are also available from the UTfit collaboration [23]).

4.1.2 Lifetime ratio

The lifetimes of the B_d and the B_s meson are measured quite precisely. The Heavy Flavor Averaging Group (HFLAV) quotes [42]:

$$\frac{\tau(B_s)}{\tau(B_d)} = 0.993 \pm 0.004\,, \quad \tau_{B_s} = (1.509 \pm 0.004)\,\text{ps}\,. \tag{4.1}$$

The non-perturbative matrix elements of the $\Delta B = 0$ operators were determined recently in [30] with Heavy Quark Effective Field Theory (HQET) sum rules, using the following notation:

$$\langle B_s|Q_i|B_s\rangle = A_i f_{B_s}^2 M_{B_s}^2 B_i\,, \quad \langle B_s|T_i|B_s\rangle = A_i f_{B_s}^2 M_{B_s}^2 \epsilon_i\,, \tag{4.2}$$

Parameter	Value	Reference
$\alpha_s(M_Z)$	0.1181(11)	PDG 2018 [48]
M_{K_S}	0.497611(13) GeV	PDG 2018 [48]
$M_{J/\psi}$	3.096900(6) GeV	PDG 2018 [48]
M_{B_d}	5.27955(26) GeV	PDG 2018 [48]
M_{B_s}	5.36684(30) GeV	PDG 2018 [48]
$\bar{m}_b \equiv m_b(m_b)$	$4.18^{+0.04}_{-0.03}$ GeV	PDG 2018 [48]
$m_{c,\text{pole}}$	1.67(7) GeV	PDG 2018 [48]
$m_c(\bar{m}_b)$	0.92(3) GeV	from $m_{c,\text{pole}}$ and $\alpha_s(M_Z)$ via RunDec [53, 54]
$m_s(\bar{m}_b)$	80^{+8}_{-6} MeV	from $m_s(2\,\text{GeV})$ [48] and $\alpha_s(M_Z)$ via RunDec
$|V_{ub}/V_{cb}|$	$0.08835^{+0.00221}_{-0.00281}$	CKMfitter [22] (ICHEP 2018 update)
V_{cb}	$0.04240^{+0.00030}_{-0.00115}$	CKMfitter [22] (ICHEP 2018 update)
V_{us}	$0.2254745^{+0.000254}_{-0.000059}$	CKMfitter [22] (ICHEP 2018 update)
γ	$65.81^{+0.99}_{-1.66}{}^{\circ}$	CKMfitter [22] (ICHEP 2018 update)

Table 2: List of input parameters needed for our theoretical predictions.

with the coefficients

$$A_1 = 1\,, \quad A_2 = \frac{M_{B_s}^2}{(m_b + m_s)^2}\,. \tag{4.3}$$

We use the following numerical values for the decay constant from the Flavour Lattice Averaging Group (FLAG) [55] and bag parameters from [30]:

$$f_{B_s} = (227.2 \pm 3.4)\,\text{MeV}, \tag{4.4}$$

$$B_1(\bar{m}_b) = 1.028^{+0.064}_{-0.056}\,, \quad B_2(\bar{m}_b) = 0.988^{+0.087}_{-0.079}\,, \tag{4.5}$$

$$\epsilon_1(\bar{m}_b) = -0.107^{+0.028}_{-0.029}\,, \quad \epsilon_2(\bar{m}_b) = -0.033^{+0.021}_{-0.021}\,, \tag{4.6}$$

where $\bar{m}_b = m_b(m_b)$. The tilded bag factors defined in Section 3.1 expressed in terms of these as follows:

$$\widetilde{B}_{1,2} = 2\epsilon_{1,2} + \frac{B_{1,2}}{N_c} \tag{4.7}$$

For the SM value of the lifetime ratio we use the prediction from [30]

$$\frac{\tau(B_s)}{\tau(B_d)} = 0.9994 \pm 0.0025\,. \tag{4.8}$$

4.1.3 B_s mixing

HFLAV quotes for the decay rate difference of B_s-mesons, $\Delta\Gamma_s$ and the semi-leptonic CP asymmetry a_{sl}^s [42]

$$\Delta\Gamma_s^{\text{exp}} = (0.088 \pm 0.006)\,\text{ps}^{-1}\,, \quad a_{sl}^{s,\text{exp}} = (-60 \pm 280) \times 10^{-5}\,. \tag{4.9}$$

For the $\Delta B = 2$ matrix elements we use [33, 55]

$$f_{B_s}\sqrt{\hat{B}} = (270 \pm 16)\,\text{MeV}\,, \quad \hat{B} = 1.32 \pm 0.06\,, \quad \frac{\tilde{B}_s(\overline{m}_b)}{B(\overline{m}_b)} = 1.07 \pm 0.06\,. \tag{4.10}$$

The renormalization-group-invariant bag parameter $\hat{B}$ can be expressed in terms of the bag parameter B from (3.20) as [55]

$$\hat{B} = (\alpha_s(\mu))^{-\frac{\gamma_0}{(2\beta_0)}} \left\{ 1 + \frac{\alpha_s(\mu)}{4\pi} \left[\frac{\beta_1\gamma_0 - \beta_0\gamma_1}{2\beta_0^2} \right] \right\} B(\mu) \tag{4.11}$$

for $m_b < \mu < m_t$, and with $N_f = 5$, and $N_c = 3$, $\gamma_0 = 4, \beta_0 = \frac{23}{3}, \gamma_1 = \frac{116}{3}, \beta_1 = -\frac{43}{9}$. We follow [33] and use

$$\hat{B} = 1.51599 \, B(m_b) \,. \tag{4.12}$$

For the SM value of the mixing observables we use [33]

$$\Delta\Gamma_s^{\text{SM}} = (0.088 \pm 0.020)\,\text{ps}^{-1} \,, \quad a_{sl}^{s,\text{SM}} = (2.22 \pm 0.27) \times 10^{-5} \,. \tag{4.13}$$

4.1.4 $B \to X_s\gamma$

For the inclusive radiative B_s meson decay we use the experimental average obtained by HFLAV [42] and the theoretical prediction from Misiak et al. [41]:

$$\mathcal{B}(\bar{B} \to X_s\gamma)^{\text{exp}} = (3.32 \pm 0.15) \times 10^{-4} \,, \tag{4.14}$$

$$\mathcal{B}(\bar{B} \to X_s\gamma)^{\text{SM}} = (3.36 \pm 0.23) \times 10^{-4}. \tag{4.15}$$

The semi-leptonic branching ratio and the ratio C as defined in Section 3.3 are taken from [45]:

$$\mathcal{B}(\bar{B} \to X_c e\bar{\nu})^{\text{exp}} = 0.1061 \pm 0.0017 \,, \tag{4.16}$$

$$C = 0.580 \pm 0.016 \,. \tag{4.17}$$

The SM contribution to $B \to X_s\gamma$ which interferes with our BSM contribution is given by [56]

$$C_{7\gamma}^{\text{eff,SM}}(m_b) = -0.385 \,. \tag{4.18}$$

4.1.5 Rare decays from BSM operators

In light of the recent anomalous measurements of $b \to s\ell\ell$ decays by LHCb, in particular the $R_{K^{(*)}}$ results [5, 57, 58] there has been considerable work on fitting the semileptonic and radiative Wilson coefficients to data. While $R_{K^{(*)}}$ are indicative of a lepton-flavour-non-universal NP effect, a UV completion of the EFT will, in general, also include a lepton-flavour-universal effect. Such a combined scenario has been shown to be consistent with (and even mildly preferred by) the data in [59] (see also [60–62]). In [1], we have studied the possible C_{9V} effects generated by $C_1^c \ldots C_4^c$ in detail. In the presence of the operators $C_i^{c\prime}$ involving right-handed strange quarks, the CBSM scenario produces an effect in C_{9V}' as well, associated with the right-handed semileptonic operator Q_{9V}'. We will treat $C_9'^{\text{eff,BSM}}(q^2, \mu)$ in (3.36) as a pseudo-observable and use the below value taken from the fit in [62] to constrain our model

$$C_9'^{\text{eff,BSM,exp}} = 0.09 \pm 0.15 \,. \tag{4.19}$$

Similarly, rare and radiative b decays can receive CBSM contributions via the coefficient $C'_{7\gamma}$ of the right-handed dipole operator $Q'_{7\gamma}$. We treat $\bar{C}'^{\text{eff}}_{7\gamma}(q^2, \mu)$ in (3.33) as a second pseudo-observable, with our experimental value value taken from the fit in [63],

$$\bar{C}'^{\text{eff,exp}}_{7\gamma} = 0.018 \pm 0.037. \tag{4.20}$$

Recall that we take $q^2 = 5\text{GeV}^2$ in $C'^{\text{eff,BSM}}_9$ and $q^2 = 0$ in $\bar{C}'^{\text{eff}}_{7\gamma}$. We have identified $C'^{\text{eff}}_9 = C'^{\text{eff,BSM}}_9$ and $C'^{\text{eff}}_{7\gamma} = \bar{C}'^{\text{eff}}_{7\gamma}$ due to the negligible SM contributions.

4.1.6 Observables in $B_d \to J/\psi K_S$

For the decay $B_d \to J/\psi K_S$ we take the CP violating observables

$$S_{J/\psi K_S} = 0.699 \pm 0.017 \,, \quad C_{J/\psi K_S} = -0.005 \pm 0.015 \,, \tag{4.21}$$

from [42], and the branching ratio

$$\mathcal{B}(B_d \to J/\psi K_S) = (8.73 \pm 0.32) \times 10^{-4} \,, \tag{4.22}$$

from [48]. As part of our theoretical calculation of $S_{J/\psi K_S}$ and $C_{J/\psi K_S}$, we use the most recent CKMfitter [22] value

$$\sin 2\beta = 0.738^{+0.027}_{-0.030} \,, \tag{4.23}$$

where the experimental measurement is not included in their fit. We note there is a very slight tension between the HFLAV average and the CKMfitter result, at the level of $\sim 1.1\,\sigma$.

For the non-perturbative decay constant of the J/ψ resonance, we take the value from the phenomenological study in [64]

$$f_{J/\psi} = (407 \pm 6)\,\text{MeV} \,. \tag{4.24}$$

This value agrees well with the lattice determinations in [64–66]. The form factor can be determined via LCSR [67] or extrapolated from lattice simulations [68, 69]. Both approaches have similar uncertainties, the LCSR values are slightly larger than the lattice results.

$$F^{B \to K}(q^2 = M^2_{J/\psi}) = 0.68 \pm 0.06 \quad \text{LCSR} \,, \tag{4.25}$$

$$F^{B \to K}(q^2 = M^2_{J/\psi}) = 0.59 \pm 0.06 \quad \text{lattice (Fermilab/MILC)} \,, \tag{4.26}$$

$$F^{B \to K}(q^2 = M^2_{J/\psi}) = 0.59 \pm 0.06 \quad \text{lattice (HPQCD)} \,. \tag{4.27}$$

4.2 Constraints on $\Delta C_5 - \Delta C_{10}$ and $\Delta C'_1 - \Delta C'_{10}$

In this section, we consider constraints upon real Wilson coefficients of operators $Q^c_5 - Q^c_{10}$ and primed operators $Q'^c_1 - Q'^c_{10}$. To determine confidence intervals for individual Wilson coefficients, we switch on BSM contributions in one Wilson coefficient at a time and set all others to their SM values. We construct a χ^2 test statistic from the experimental measurements of our chosen observables and our theoretical predictions, combining the experimental and theoretical errors in quadrature[7]:

$$\chi^2_i(\vec{C}^c) = \frac{\left(\mathcal{O}^{\text{th}}_i(\vec{C}^c) - \mathcal{O}^{\text{exp}}_i\right)^2}{(\sigma^{\text{exp}}_i)^2 + (\sigma^{\text{th}}_i)^2} \,, \tag{4.28}$$

---

[7] We make the assumption that the experimental and theoretical errors are Gaussian distributed and independent.

where the index i runs over $\mathcal{B}(\bar{B} \to X_s \gamma)$, $\Delta\Gamma_s$ and $\frac{\tau(B_s)}{\tau(B_d)}$ and in addition our "pseudo-observables" $\bar{C}_{7\gamma}'^{\text{eff}}(q^2,\mu)$ and $C_9'^{\text{eff,BSM}}(q^2,\mu)$. The 1σ intervals implied by individual observables are displayed in Tables 3 and 4. To obtain combined constraints (Table 5), we sum up the individual χ^2. In all cases we normalise to the best fit value by subtracting the relevant χ^2 value at the minimum, $\Delta\chi^2 = \chi^2 - \chi^2_{\min}$.

Coeff.	$\Delta\chi^2_\gamma \leq 1$	$\Delta\chi^2_\tau \leq 1$	$\Delta\chi^2_{\Delta\Gamma} \leq 1$
ΔC_5	$[-0.01, 0.01], [0.36, 0.37]$	$[-0.03, -0.01], [0.03, 0.06]$	$[-0.13, 0.34]$
ΔC_6	$[-0.02, 0.03], [1.1, 1.2]$	$[-0.11, -0.03], [0.09, 0.17]$	$[-1.5, 0.49]$
ΔC_7	$[-0.46, -0.45], [-0.01, 0.01]$	$[-0.21, -0.11], [0.04, 0.14]$	$[-1.7, 0.44]$
ΔC_8	$[-0.92, -0.88], [-0.02, 0.014]$	$[-0.26, -0.12], [0.06, 0.20]$	$[-0.27, 0.27]$
ΔC_9	$[-0.002, 0.003], [0.15, 0.15]$	$[-0.02, -0.01], [0.003, 0.011]$	$[-0.14, 0.035]$
ΔC_{10}	$[-0.05, 0.07], [3.2, 3.3]$	$[-0.08, -0.05], [0.02, 0.05]$	$[-0.09, 0.09]$
$\Delta C_1'$	$[-5.7, 5.7]$	$[-0.32, -0.15], [0.08, 0.25]$	$[-0.58, 0.58]$
$\Delta C_2'$	$[-0.53, 0.53]$	$[-1.2, -0.51], [0.39, 1.1]$	$[-0.39, 0.39]$
$\Delta C_3'$	$[-6.7, 6.7]$	$[-1.0, -0.79], [0.06, 0.30]$	$[-1.1, 1.1]$
$\Delta C_4'$	$[-0.75, 0.75]$	$[-1.3, -0.96], [0.09, 0.45]$	$[-0.44, 0.44]$
$\Delta C_5'$	$[-0.05, 0.05]$	$[-0.03, -0.01], [0.03, 0.06]$	$[-0.21, 0.21]$
$\Delta C_6'$	$[-0.15, 0.15]$	$[-0.10, -0.03], [0.10, 0.18]$	$[-0.85, 0.85]$
$\Delta C_7'$	$[-0.06, 0.06]$	$[-0.23, -0.13], [0.03, 0.13]$	$[-0.86, 0.86]$
$\Delta C_8'$	$[-0.12, 0.12]$	$[-0.30, -0.17], [0.04, 0.17]$	$[-2.0, 2.0]$
$\Delta C_9'$	$[-0.02, 0.02]$	$[-0.02, -0.01], [0.003, 0.011]$	$[-0.07, 0.07]$
$\Delta C_{10}'$	$[-0.42, 0.42]$	$[-0.09, -0.05], [0.01, 0.05]$	$[-1.2, 1.2]$

Table 3: 1σ intervals for scenarios with one Wilson coefficient.

Coeff.	$\Delta\chi^2_{C_9'^{\text{eff,BSM}}} \leq 1$	$\Delta\chi^2_{\bar{C}_{7\gamma}'^{\text{eff}}} \leq 1$
$\Delta C_1'$	$[-0.01, 0.02]$	$[-1.10, 3.2]$
$\Delta C_2'$	$[-0.02, 0.11]$	$[-0.30, 0.10]$
$\Delta C_3'$	$[-0.04, 0.01]$	$[-3.7, 1.3]$
$\Delta C_4'$	$[-0.08, 0.02]$	$[-0.42, 0.14]$
$\Delta C_5'$	$-$	$[-0.01, 0.03]$
$\Delta C_6'$	$-$	$[-0.03, 0.08]$
$\Delta C_7'$	$-$	$[-0.03, 0.01]$
$\Delta C_8'$	$-$	$[-0.07, 0.02]$
$\Delta C_9'$	$-$	$[-0.004, 0.01]$
$\Delta C_{10}'$	$-$	$[-0.08, 0.23]$

Table 4: 1σ intervals for scenarios with one primed Wilson coefficient. These correspond to allowed ranges for $\bar{C}_{7\gamma}'^{\text{eff}}$ and $C_9'^{\text{eff,BSM}}$ at $\pm 1\sigma$.

Considering $\Delta C_5 - \Delta C_{10}$ in the first column of Table 3, there are best fit ranges which correspond to those that pass through the SM point and those that do not. This can be understood by considering the functional form with which $\bar{C}_{7\gamma}^{\text{eff}}$ enters (3.31) and the impact that larger contributions from coefficients in $C_{7\gamma}^{\text{eff, BSM}}$ have upon reducing the parameter space allowed by radiative decay. The second column of Table 3 does not for any coefficient include the SM point, and this is simply due to the current disagreement between measurement and theory for the lifetime ratio. Column 3 containing ranges accommodated by $\Delta\Gamma_s$ always includes the SM point. In Table 4 we show 1σ ranges for the primed coefficients, accommodated by pseudo observables $C_9^{\prime\text{eff,BSM}}$ and $\bar{C}_{7\gamma}^{\prime\text{eff}}$. In the second column of Table 5 we show the 1σ allowed ranges for $\Delta C_5 - \Delta C_{10}$ which follow from from combining constraints of all observables. The 1σ ranges for the primed coefficients $\Delta C_1' - \Delta C_{10}'$ however exclude the radiative decay branching ratio observable, as this is already contained in the fitted value of $\bar{C}_{7\gamma}^{\prime\text{eff,exp}}$. In the last two columns of Table 5 we re-express the combined bounds in terms of the scale of new physics Λ_{NP}, defined through

$$\frac{4G_F}{\sqrt{2}}|V_{cb}V_{cs}^*||\Delta C_i| = \frac{1}{\Lambda_{\text{NP}}^2}. \tag{4.29}$$

The lower bound on the NP scale corresponding to the negative boundary of the 1σ interval for ΔC_i is denoted as Λ_-, that corresponding to the positive boundary as Λ_+. For ΔC_{10} and $\Delta C_9'$ the 1σ interval only contains positive values and only Λ_+ is given, corresponding to the upper boundary. For $\Delta C_{10}'$, the 1σ region is composed of two interval, and Λ_- and Λ_+ correspond to the smallest and largest Wilson coefficient values (-0.08 and 0.05, respectively). We see that with our definition of Λ_{NP}, which is agnostic to the details of BSM physics generating the ΔC_i^c, our observables can provide sensitivity to scales higher than 20 TeV in scenarios involving the tensor Wilson coefficient $\Delta C_9^{(\prime)}$. Other Wilson coefficients probe somewhat lower scales, but always at least 3 TeV.

For scenarios in which we consider NP in pairs of Wilson coefficients, setting all others to their SM values; the pattern of constraints may be divided into three categories:

(i) Coefficients $\Delta C_5 - \Delta C_{10}$: As explained in Section 2.2, the mixing of operators $Q_5^c, ..., Q_{10}^c$ with $Q_{7\gamma}$ first at one-loop gives rise to strong RG effects which enter $\bar{C}_{7\gamma}^{\text{eff}}$ and result in the dominant constraint for such scenarios coming from radiative decay. As the coefficient $\bar{C}_{7\gamma}^{\text{eff}}$ enters (3.31) both quadratically as well as linearly, it receives a contribution from $C_{7\gamma}^{\text{eff,SM}}$. This combination results in a much narrower 1 sigma region, as is shown in all panels of Figure 2 as the blue shaded area. In the first and third panel, the presence of another purple band corresponds to contours where $\bar{C}_7^{\text{eff}} = -2C_{7\gamma}^{\text{eff,SM}}$. In terms of the lifetime ratio, shown in the green shaded area, the contours slightly miss the SM point due to the current 1.4σ discrepancy between theory and experiment. For the $B_s - \bar{B}_s$ width difference the scenarios consisting of coefficients of operators with left and right handed vector currents and coefficients of tensor operators are the most restrictive. In all cases scenarios between even numbered coefficients are favoured owing to the $\frac{1}{N_c}$ suppression which always accompanies colour singlet operators in the calculations.

Coeff.	$\Delta\chi^2 \leq 1$	Λ_-(TeV)	Λ_+(TeV)
ΔC_5	$[-0.01, 0.01]$	9.7	10.5
ΔC_6	$[-0.02, 0.02]$	5.6	5.8
ΔC_7	$[-0.01, 0.01]$	8.8	9.7
ΔC_8	$[-0.02, 0.02]$	6.2	6.9
ΔC_9	$[-0.001, 0.01]$	22.3	12.6
ΔC_{10}	$[0.01, 0.05]$	-	3.8
$\Delta C_1'$	$[-0.01, 0.02]$	11.9	5.5
$\Delta C_2'$	$[-0.04, 0.09]$	4.5	2.8
$\Delta C_3'$	$[-0.04, 0.02]$	4.5	7.0
$\Delta C_4'$	$[-0.07, 0.03]$	3.2	5.1
$\Delta C_5'$	$[-0.02, 0.04]$	5.8	4.5
$\Delta C_6'$	$[-0.07, 0.11]$	3.3	2.6
$\Delta C_7'$	$[-0.03, 0.02]$	5.1	6.6
$\Delta C_8'$	$[-0.06, 0.04]$	3.6	4.3
$\Delta C_9'$	$[0.002, 0.010]$	-	8.5
$\Delta C_{10}'$	$[-0.08, -0.06], [0.02, 0.05]$	3.1	3.8

Table 5: Allowed 1σ ranges from all observables combined and corresponding bounds on BSM scale.
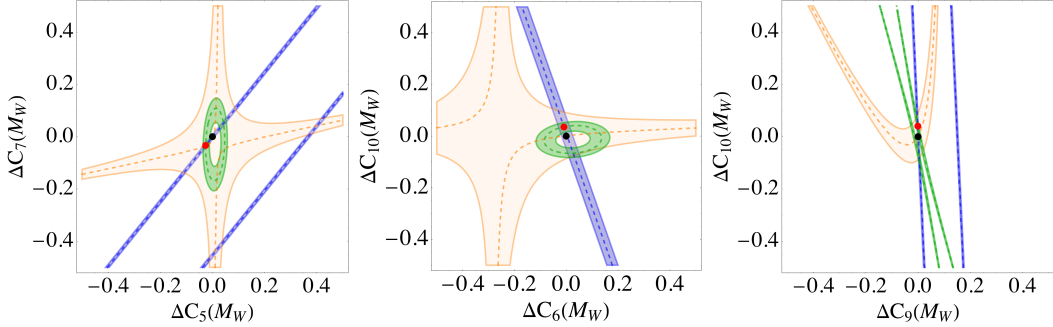
Figure 2: Overlaid individual constraints from radiative decay (blue), lifetime ratio (green), width difference (orange) upon $\Delta C_5 - \Delta C_7$ plane (left), $\Delta C_6 - \Delta C_{10}$ plane (middle), $\Delta C_9 - \Delta C_{10}$ plane (right). The SM point and best fit point are shown as the black and red dots respectively.

(ii) $\Delta C_1' - \Delta C_4'$: The 6 plots in Figure 3 show as additional constraints, contours of $C_9'^{\text{eff,BSM}} = 0.09 \pm 0.15$ and of $\bar{C}_{7\gamma}'^{\text{eff}} = 0.018 \pm 0.037$ in 2 parameter planes of Wilson coefficients $\Delta C_1'(M_W) - \Delta C_4'(M_W)$. Here the central value used is the best fit points for C_{9V}' and $C_{7\gamma}'$ acquired from global fits to angular observables in [62], [63]. These are to be compared with the high scale scenarios considered already in [1] and discussed in Section 4.3. For combinations of these coefficients it is found that the strongest
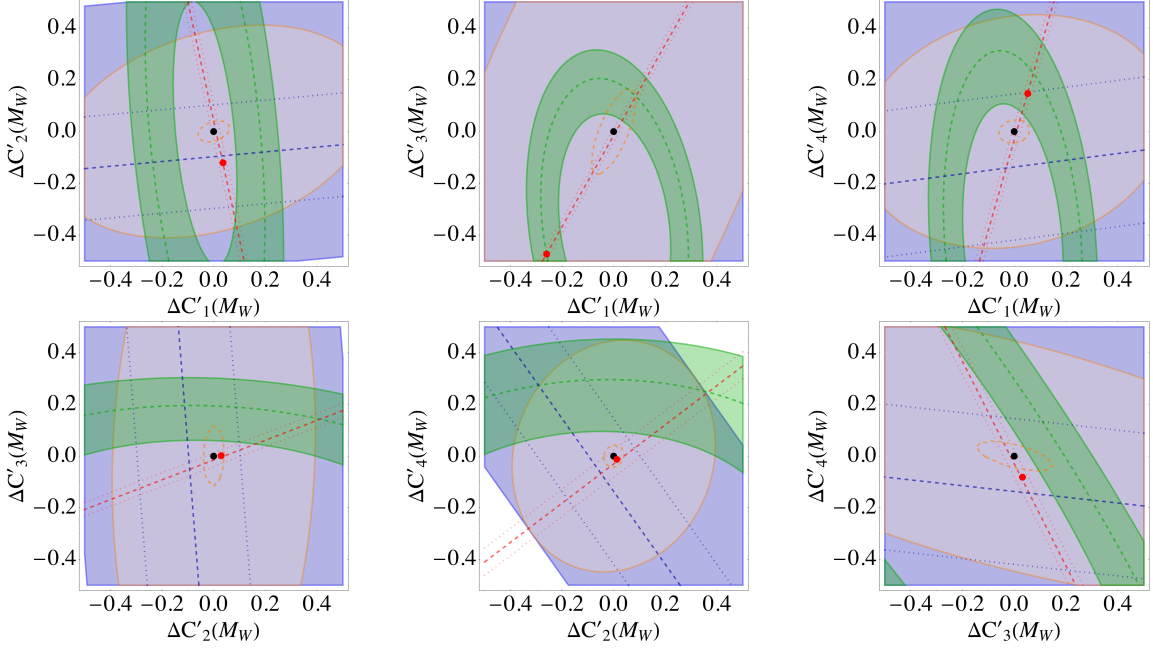
Figure 3: Contours of $C_9^{\prime\text{eff,BSM}} = 0.09 \pm 0.15$ (red, dashed) and of $\bar{C}_{7\gamma}^{\prime\text{eff}} = 0.018 \pm 0.037$ (blue, dashed), along with radiative decay (blue), lifetime ratio (green) and width difference (orange) 1σ constraints upon two parameter scenarios involving Wilson coefficients $\Delta C_1^{\prime} - \Delta C_4^{\prime}$. The SM point and best fit point are shown as the black and red dots respectively.

constraint comes from the experimental fits of angular observables to $C_{9V}^{\prime}$. This is due to a strong dependence of $C_{9V}^{\prime\text{BSM}}(m_b)$ upon $\Delta C_1^{\prime}(M_W) - \Delta C_4^{\prime}(M_W)$ which results in closely spaced contours (red dashes). The inclusive radiative decay branching ratio constraint (blue shading) is shown for extra information, in addition to that given by the contours of $\bar{C}_{7\gamma}^{\prime\text{eff}}$ at fitted value of $\bar{C}_{7\gamma}^{\prime\text{eff,exp}}$ (which includes inclusive branching ratio data). For these primed coefficients the radiative decay constraint is very much weaker than in the previous case due to the mixing of operators $Q_1^{c\prime}, ..., Q_4^{c\prime}$ with $Q_{7\gamma}^{\prime}$ occurring first at two-loop, and in addition, to the primed coefficient $\bar{C}_{7\gamma}^{\prime\text{eff}}$ only entering (3.31) quadratically with no linear dependence upon $C_{7\gamma}^{\text{eff,SM}}$.

(iii) $\Delta C_5^{\prime} - \Delta C_{10}^{\prime}$: Three examples of possible 2 parameter scenarios are shown in Figure 4 and are the right handed counter parts in one to one correspondence with those of Figure 2. As in (i) the one-loop mixing under renormalization of $Q_5^{c\prime}, ..., Q_{10}^{c\prime}$ with $Q_{7\gamma}^{\prime}$ results in a stronger dependence of $\bar{C}_{7\gamma}^{\prime\text{eff}}$ upon $\Delta C_5^{\prime} - \Delta C_{10}^{\prime}$ and this results in strict constraints upon combinations of these coefficients. All plots show very similar constraints from the lifetime ratio and the width difference, although differences are more pronounced in $\Delta\Gamma_s$ due to primed and unprimed coefficients not mixing in the theoretical prediction for $\Gamma_{12}^{c\bar{c}}$ and hence there is no linear contribution from SM parts of Wilson coefficients C_1^c and C_2^c here. The best fit points shown in red are all placed close to the SM point (black), but are pulled away slightly by the lifetime ratio constraint.
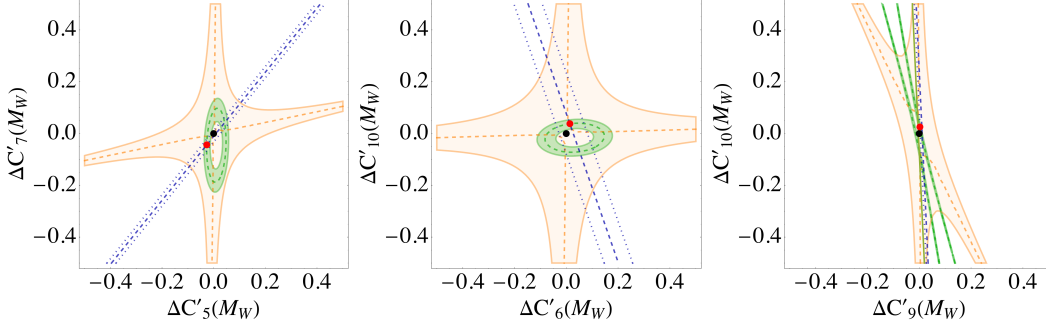
Figure 4: Overlaid individual constraints upon $\bar{C}_{7\gamma}^{\prime\text{eff}}$ (blue dashed central value/dotted $\pm\sigma$), lifetime ratio (green), width difference (orange) upon $\Delta C_5' - \Delta C_7'$ plane (left), $\Delta C_6' - \Delta C_{10}'$ plane (middle), $\Delta C_9' - \Delta C_{10}'$ plane (right). The SM point and best fit point are shown as the black and red dots respectively.

4.3 The case of $\Delta C_1 - \Delta C_4$

For the case of the C_{1-4}^c, the phenomenology for a scenario with purely real coefficients was covered in our previous paper [1] – we briefly recap our conclusions from that work, before expanding to a scenario with complex coefficients and the constraints that arise from $B_d \to J/\psi K_S$ decays. Complex NP in C_1^c and C_2^c will be studied in the upcoming work [70] – where they compute constraints arising from $\tau(B_s)/\tau(B_d)$ and $\mathcal{B}(B \to X_s\gamma)$ as part of a sophisticated global fit. We performed a mutual check with the authors of that work, and found full agreement on the constraints arising from the previously mentioned observables (i.e. the blue and green bands in Figure 5 below).

In [1], we studied NP confined to the first four operators of the full basis (2.3), as these operators give a large contribution to a (lepton flavour universal) shift in the C_{9V} coefficient (since the RG running coefficients are $\mathcal{O}(1/\alpha_s)$ in the logarithmic counting), while only being constrained by the radiative decays through two-loop RG mixing. In our study we found that while the SM is consistent with the lifetime ratio, width difference and radiative decay observables, there is also room for a shift in our $(\bar{c}b)(\bar{s}c)$ Wilson coefficients without disagreement with data – see Fig. 3 in [1]. For instance, a shift to the C_3^c coefficient alone of order 0.2 could produce a shift of C_{9V} of order -1, and such an NP contribution is in fact slightly favoured with respect to the Standard Model, as it lessens the small tension present in $\tau(B_s)/\tau(B_d)$. NP in two coefficients simultaneously can also be accommodated, such as in the pair $(\Delta C_2, \Delta C_4) = (-0.1, 0.3)$ which generates an $\mathcal{O}(1)$ contribution to C_{9V} (albeit with no change relative to the SM in the lifetime ratio). In light of the fact that current data supported a possible NP contribution in several different Wilson coefficients, the natural question was how to distinguish between these scenarios. We showed that an improvement in the future precision of both the lifetime ratio and the width difference $\Delta\Gamma_s$ could identify the particular realisation of charming BSM physics in nature.

As introduced in Section 3.5, NP in $(\bar{c}b)(\bar{s}c)$ operators can alter the $B_d \to J/\psi K_S$ decay rate, as well as the related CP asymmetries $S_{J/\psi K_S}$ and $C_{J/\psi K_S}$ in the case of complex Wilson coefficients. In order to predict these three observables, hadronic operator

matrix elements $\langle J/\psi K_S | O_i^c | \bar{B} \rangle$ must be evaluated. In the SM, the NF approximation for them does not give good agreement data, and it is widely assumed that deviations from NF can bring the prediction in line with experiment; as reviewed in Section 3.5, large deviations from naive factorization are theoretically to be expected for $\langle O_2^c \rangle$ but not $\langle O_1^c \rangle$.

However, in this section we jointly consider the three observables, to constrain either ΔC_1 or ΔC_2 together with the uncertain matrix element ratio r_{21} defined in Section 3.5, with the matrix element $\langle O_1 \rangle$, for which violations of NF are expected to be small, taken in the range described there. Constructing a χ^2 test statistic out of the three observables and the $\langle O_1 \rangle$ range and profiling it over $\langle O_1 \rangle$ and r_{21} results in a constraint in the complex $\Delta C_{1,2}$ planes.

For the complex ΔC_1 plane, the resulting constraint is shown in Figure 5 (left) as red bands, implying a remarkably powerful constraint from this hadronic decay: the imaginary part must be close to either zero or ± 0.2. In effect, we have determined the uncertain matrix element ratio r_{21} from data. We show in the figure the 1, 2, and 3σ regions for the $B_d \to J/\psi K_S$ constraints. The $\text{Im}\, C_1 = 0$ band is very narrow, and has no 1σ region because of the slight discrepancy for $\sin 2\beta$ mentioned in Section 4.1.6. In the same figure we overlay the constraints from a_{sl}^s (yellow), $\Delta\Gamma_s$ (orange), and $\tau(B_s)/\tau(B_d)$ (green). We see that the lifetime ratio is the most constraining among the three, while the other two rule out some regions with larger real and/or imaginary NP contributions ($B \to X_s\gamma$ provides no visible constraints at this scale). Combined with the constraint from $B \to J/\psi K_S$, only a few small regions in the ΔC_1 plane are allowed.

In fact, the χ^2-profiling allows, at each point in the plane, to simultaneously determine the value of r_{21} that gives the best fit. For reasons of computational simplicity, we carry this out only along a circle in the middle of the (green) lifetime ratio ring, where the experimental central value of $\tau(B_s)/\tau(B_d)$ is obtained. Along this ring, the (complex) value of r_{21} varies substantially. Along the two short black segments it is in excellent agreement with naive factorization. Surprisingly, these two segments happen to lie in two of the small regions in the plane that are allowed by all constraints. We have no explanation for this curious fact. But it certainly demonstrates that experimental data in $B \to J/\psi K_S$ does *not* imply large violations of naive factorization, in contrast to a widely held belief. (Similar results are found when varying the radius of the circle within the lifetime band, corresponding to different fixed values of $\tau(B_s)/\tau(B_d)$.)

The results of repeating the study for complex ΔC_2 are displayed in Figure 5 (right). In this case, $B_d \to J/\psi K_S$ data allows a band centred on the real, as well as a second band with negative real and imaginary parts that however is ruled out by the other constraints; among those, the most stringent constraints now come from the lifetime difference $\Delta\Gamma_s$ and the radiative decay $B \to X_s\gamma$. Extending beyond the SM operators $Q_{1,2}^c$ to NP in $Q_{3,4}^c$, the theoretical prediction for $B_d \to J/\psi K_S$ requires more non-perturbative inputs in the form of r_{31}, r_{41}, alongside r_{21} (as there is still a SM contribution to C_2^c). Attempting to fit these from the $B_d \to J/\psi K_S$ data does not bring any further insight, as there is sufficient freedom to always explain the measurements.
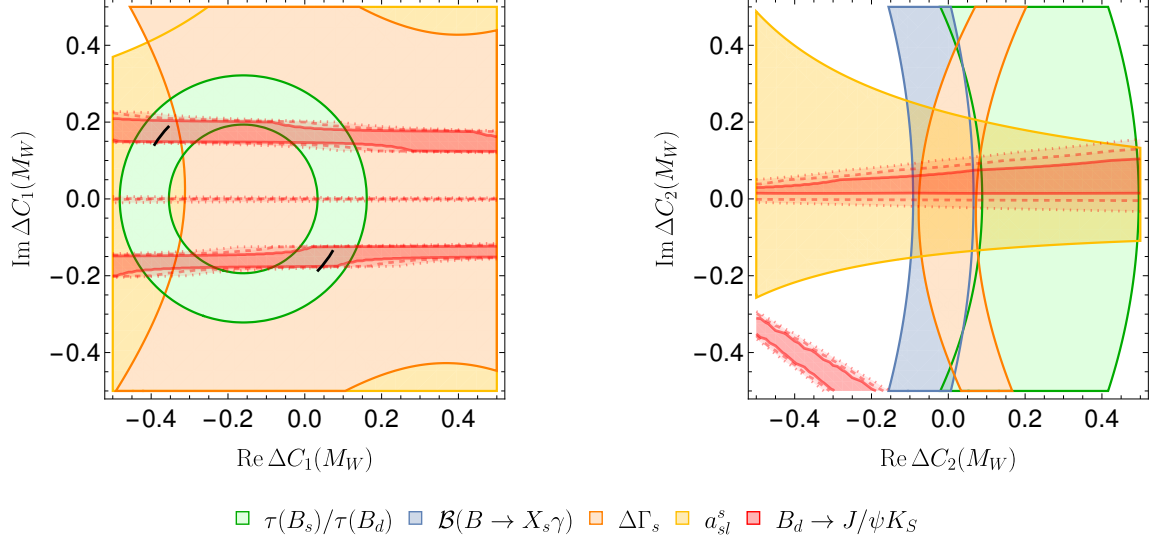
Figure 5: Left: Constraints from $B_d \to J/\psi K_S$ and other constraints on the complex ΔC_1 plane. The red horizontal bands uses a theory prediction only for $\langle O_1 \rangle$, expected to be close to its naive-factorization value as reviewed in Section 3.5. Each band shows regions of agreement at the 1σ (solid), 2σ (dashed), and 3σ (dotted) levels. (Note that the band lying on the real axis only has 2 and 3σ agreement, due to the small tension between (4.21) and (4.23)). On the black arcs, NF for both $\langle O_1^c \rangle$ and r_{21} is in agreement with data. Right: Same, but for NP in ΔC_2.

5 Conclusions

In this paper we have made a thorough study of the possible effects of new physics arising in tree-level $b \to c\bar{c}s$ decays. This partonic decay mode contributes to a wide variety of different observables. Among them, the branching ratio for radiative B meson decay $\mathcal{B}(B \to X_s\gamma)$, the B meson lifetime ratio $\tau(B_s)/\tau(B_d)$, and the B_s mixing observables $\Delta\Gamma_s$ and a_{sl}^s stand out: They are inclusive decay modes that are well measured experimentally, and are theoretically controlled through the HQE. In addition, we have shown that, in the CP-violating case, new constraints which are only midlly affected by theoretical uncertainties arise from exclusive $B_d \to J/\psi K_S$ observables. Taken together, effects in this set of observables are correlated in our "Charming BSM" scenario, and the observables provide very complementary constraints on it.

The space of NP contributing to $b \to c\bar{c}s$ decays is spanned by 20 operators, defined in (2.3). We have calculated the contribution from the full basis to all of our observables; the most complex result being that obtained for mixing and the lifetime ratio for which we used tools from the Mathematica package FeynCalc [71, 72]. Our full results are given in (3.19)–(3.23) and (3.4)–(3.14) (these results are also available as ancillary `Mathematica` files with arXiv version of this article). We have further calculated the renormalization group evolution for our basis. In the SM case we used known results for ADM entries available in the literature [18, 28] and for the mixing of our operators as described in Section 2.2,

elements from [26], our previous work [1], as well as those elements extracted from our $b \rightarrow s\ell\ell$ results either directly or through substitution of relevant colour factors. Our results are summarised in the full evolution matrix given in (2.25). An explicit recipe for making use of our results to place constraints on an arbitrary NP model is as follows:

1. Match the chosen BSM model onto our effective Hamiltonian (given in (2.2)) at the scale M_W.

2. Use the RG evolution matrix (given in (2.25)) to run the effective coefficients down to the scale m_b.

3. Use the low scale Wilson coefficients as inputs to the algebraic expressions for the observables $\Delta\Gamma_s$ (given in (3.19)–(3.23), or the attached file `Gamma12.m`), $\tau(B_s)/\tau(B_d)$ (given in (3.4)–(3.14), or the attached file `LifetimeRatio.m`), and $\mathcal{B}(B \rightarrow X_s\gamma)$ (given in (3.27)–(3.34)), to generate BSM theory predictions in terms of the BSM theory parameters.

4. Compare the computed BSM theory predictions to the corresponding experimental measurements of choice.

We have extended our earlier results [1] in two important ways. Firstly, we complement our previous analysis of real new physics in Q^c_{1-4} by studying the possibility of CP-violating NP, and introduced observables from $B_d \rightarrow J/\psi K_S$ as constraints. Secondly, we studied constraints from our main set of observables on the Wilson coefficients $C^{c(\prime)}_{5-10}$ and in analogy with our study of C^c_{1-4} we have constrained from global fits to the "wrong chirality" coefficients C'_{9V} and $C'_{7\gamma}$, possible BSM effects in $C^{c(\prime)}_{1-4}$.

When considering the introduction of new weak CP violating phases to SM coefficients, we have used the sine and cosine coefficients $S_{J/\psi K_S}$ and $C_{J/\psi K_S}$ of the time dependent CP asymmetry, alongside the branching ratio $\mathcal{B}(B_d \rightarrow J/\psi K_S)$ to constrain the parameter space. By treating the uncertain hadronic matrix element ratio $r_{21} = \langle O_2 \rangle / \langle O_1 \rangle$ as a free parameter and profiling over it, we effectively determine it from data, reducing the required theoretical input to the colour-allowed matrix element $\langle O_1 \rangle$. We assume this to be close to its value in naive factorization, as is expected from large-N_C counting. In this way we obtained constraints relying only mildly on theory, even though we are dealing with nonleptonic exclusive decays.

For NP in ΔC_1, our result (shown in Figure 5) turns out to be very interesting. Firstly, the combination of inclusive and $B_d \rightarrow J/\psi K_S$ constraints only leaves a few small regions of the complex C_1 plane where agreement is obtained between the full compliment of observables and their respective experimental averages, including some where C_1 has an imaginary part of close to ± 0.2. Secondly, whereas naive factorisation is not expected to well describe class II colour suppressed decays, we find that in one of the allowed regions with complex C_1, r_{21} happens to be close to its NF prediction. This requires a small negative imaginary BSM shift $\sim -0.2i$ to C_1. When considering ΔC_2, we again observe a strong complementarity of the constraints. A broad band centred on real shifts is compatible with $B \rightarrow J/\psi K_S$ data, as well as a diagonal region with negative real and imaginary parts.

Unfortunately the other constraints we consider have no clear region of overlap where all the predictions can be brought into agreement with data, due to a mild tension between the lifetime ratio on the one hand and radiative decay and the B_s width difference on the other hand. When considering ΔC_3 and ΔC_4, there are too many non-perturbative parameters in play to obtain constraints from $B \to J/\psi K_S$.

Turning now to our results for $\Delta C_{5-10}^{(\prime)}$ and $\Delta C_{1-4}'$, we group them into three categories exhibiting similar behaviour. Consider $\Delta C_{1-4}'$, it was found that the strongest constraint upon these coefficients comes indirectly from angular observables through our displayed contours of constant $C_9'^{\text{eff,BSM}}$ at the fitted values of $C_{9V}'^{\text{exp}} \pm 1\sigma$, and to a lesser degree, contours of constant $\bar{C}_{7\gamma}'^{\text{eff}}$ at the fitted values of $\bar{C}_{7\gamma}'^{\text{exp}} \pm 1\sigma$. In all panels we would expect viable values of pairs of BSM coefficients to lie within the region bounded by these contours. We obtain no strong constraint from radiative decay for these coefficients as the small 2 loop mixing of $C_{7\gamma}'^{\text{eff}}$ with this set of coefficients in addition to the purely quadratic dependence of the branching fraction upon $\bar{C}_{7\gamma}'^{\text{eff}}$, leads to relaxed bounds. Of all the scenarios considered, we find that pairs involving $\Delta C_1' - \Delta C_3'$ and $\Delta C_1' - \Delta C_4'$ stand out as scenarios where agreement with all data can be found. Considering now ΔC_{5-10}, in contrast to the above case, the mixing of $C_{7\gamma}'^{\text{eff}}$ with ΔC_{5-10} occurs at 1-loop and results in these coefficients being very highly constrained by radiative decay, and this indicates that models involving combinations of these coefficients are disfavoured by our study. Finally, we consider the coefficients $\Delta C_{5-10}'$. These are constrained in a similar fashion to their unprimed counterparts by each of our observables except the radiative decay branching ratio, which we replace by contours of $\bar{C}_{7\gamma}'^{\text{eff}} = \bar{C}_{7\gamma}'^{\text{exp}} \pm 1\sigma$. Graphical representations of the allowed parameter space are shown in Figures 2–4.

As a step towards converting our constraints into statements on more definite NP models, we considered what the equivalent NP scale Λ_{NP} we are probing when we place limits on our Wilson coefficients, and our results were shown in Table 5. The tensor operators $Q_9^{(\prime)c}$ are sensitive to the highest scales, with the best fit to those coefficients corresponding to scales in excess of $10\,\text{TeV}$. All our operators probe scales above $2\,\text{TeV}$, showing how our choice of observables can complement direct LHC searches for NP effects.

Acknowledgments

A Explicit expressions for anomalous dimensions matrices

Note that as mentioned in Section 2.2.1, the two-loop mixing of $Q_{3,4}^c$ into the gluon penguin Q_{8g} has not been calculated – this corresponds to the zeros in the third and fourth elements of $\vec{\gamma}_{A8}^{(0)}$.

$$\hat{\gamma}_{AA} = \frac{\alpha_s}{4\pi} \begin{pmatrix} -2 & 6 & 0 & 0 & 0 & 0 \\ 6 & -2 & 0 & 0 & 0 & 0 \\ 0 & 0 & 2 & -6 & 0 & 0 \\ 0 & 0 & 0 & -16 & 0 & 0 \\ 0 & 0 & 0 & 0 & -16 & 0 \\ 0 & 0 & 0 & 0 & -6 & 2 \end{pmatrix} \tag{A.1}$$

$$\hat{\gamma}_{BB} = \frac{\alpha_s}{4\pi} \begin{pmatrix} 2 & -6 & -\frac{7}{6} & -\frac{1}{2} \\ 0 & -16 & -1 & \frac{1}{3} \\ -56 & -24 & -\frac{38}{3} & 6 \\ -48 & 16 & 0 & \frac{16}{3} \end{pmatrix} \tag{A.2}$$

$$\hat{\gamma}_{Ap} = \frac{\alpha_s}{4\pi} \begin{pmatrix} 0 & 0 & 0 & 0 \\ 0 & \frac{4}{3} & 0 & 0 \\ 0 & 0 & 0 & 0 \\ 0 & -\frac{2}{3} & 0 & 0 \\ 0 & 0 & 0 & 0 \\ 0 & 0 & 0 & 0 \end{pmatrix} \tag{A.3}$$

$$\hat{\gamma}_{pp} = \frac{\alpha_s}{4\pi} \begin{pmatrix} 0 & -\frac{52}{3} & 0 & 2 \\ -\frac{40}{9} & -\frac{100}{9} & \frac{4}{9} & \frac{5}{6} \\ 0 & -\frac{256}{3} & 0 & 20 \\ -\frac{256}{9} & \frac{56}{9} & \frac{40}{9} & -\frac{2}{3} \end{pmatrix} \tag{A.4}$$

$$\gamma_{77} = \frac{\alpha_s}{4\pi} \left(\frac{32}{3} \right) \tag{A.5}$$

$$\gamma_{87} = \frac{\alpha_s}{4\pi} \left(-\frac{32}{9} \right) \tag{A.6}$$

$$\gamma_{88} = \frac{\alpha_s}{4\pi} \left(\frac{28}{3} \right) \tag{A.7}$$

$$\vec{\gamma}_{A7} = \frac{\alpha_s}{4\pi} \left(0 \ \frac{464}{81} \ 0 \ \frac{200}{81} \ 0 \ 0 \right)^T \tag{A.8}$$

$$\vec{\gamma}_{A8} = \frac{\alpha_s}{4\pi} \left(3 \ \frac{76}{27} \ 0 \ 0 \ 0 \ 0 \right)^T \tag{A.9}$$

$$\vec{\gamma}_{p7} = \frac{\alpha_s}{4\pi} \left(\frac{64}{81} \ -\frac{200}{243} \ -\frac{6464}{81} \ -\frac{11408}{243} \right)^T \tag{A.10}$$

$$\vec{\gamma}_{p8} = \frac{\alpha_s}{4\pi} \left(\frac{368}{27} \ -\frac{1409}{162} \ \frac{13052}{27} \ -\frac{2740}{81} \right)^T \tag{A.11}$$

$$\vec{\gamma}_{p9} = \frac{\alpha_s}{4\pi} \left(-\frac{16}{9} \ \frac{32}{27} \ -\frac{112}{9} \ \frac{512}{27} \right)^T \tag{A.12}$$

$$\vec{\gamma}_{B7} = \left(\frac{2m_c}{m_b} \ \frac{2m_c}{3m_b} \ -\frac{8m_c}{m_b} \ -\frac{8m_c}{3m_b} \right)^T \tag{A.13}$$

$$\vec{\gamma}_{B8} = \left(0 \ \frac{m_c}{m_b} \ 0 \ -\frac{4m_c}{m_b} \right)^T \tag{A.14}$$

$$\vec{\gamma}_{A9} = \left(-\frac{8}{3} \ -\frac{8}{9} \ \frac{4}{3} \ \frac{4}{9} \right)^T \tag{A.15}$$

References

[1] S. Jäger, M. Kirk, A. Lenz and K. Leslie, *Charming new physics in rare B-decays and mixing?*, *Phys. Rev.* **D97** (2018) 015021 [1701.09183].

[2] C. W. Bauer and N. D. Dunn, *Comment on new physics contributions to* Γ_{12}^s, *Phys. Lett.* **B696** (2011) 362 [1006.1629].

[3] LHCB collaboration, *Differential branching fractions and isospin asymmetries of* $B \to K^{(*)}\mu^+\mu^-$ *decays*, *JHEP* **06** (2014) 133 [1403.8044].

[4] LHCB collaboration, *Angular analysis and differential branching fraction of the decay* $B_s^0 \to \phi\mu^+\mu^-$, *JHEP* **09** (2015) 179 [1506.08777].

[5] LHCB collaboration, *Search for lepton-universality violation in* $B^+ \to K^+\ell^+\ell^-$ *decays*, *Phys. Rev. Lett.* **122** (2019) 191801 [1903.09252].

[6] CMS collaboration, *Angular analysis of the decay* $B^0 \to K^{*0}\mu^+\mu^-$ *from pp collisions at* $\sqrt{s} = 8$ *TeV*, *Phys. Lett.* **B753** (2016) 424 [1507.08126].

[7] BABAR collaboration, *Measurement of angular asymmetries in the decays* $B \to K^*\ell^+\ell^-$, *Phys. Rev.* **D93** (2016) 052015 [1508.07960].

[8] BELLE collaboration, *Measurement of the Differential Branching Fraction and Forward-Backword Asymmetry for* $B \to K^{(*)}\ell^+\ell^-$, *Phys. Rev. Lett.* **103** (2009) 171801 [0904.0770].

[9] CDF collaboration, *Measurements of the Angular Distributions in the Decays* $B \to K^{(*)}\mu^+\mu^-$ *at CDF*, *Phys. Rev. Lett.* **108** (2012) 081807 [1108.0695].

[10] LHCB collaboration, *Angular analysis of the* $B^0 \to K^{*0}\mu^+\mu^-$ *decay using 3 fb^{-1} of integrated luminosity*, *JHEP* **02** (2016) 104 [1512.04442].

[11] BELLE collaboration, *Angular analysis of* $B^0 \to K^*(892)^0\ell^+\ell^-$, in *Proceedings, LHCSki 2016 - A First Discussion of 13 TeV Results: Obergurgl, Austria, April 10-15, 2016*, 2016, 1604.04042.

[12] BELLE collaboration, *Lepton-Flavor-Dependent Angular Analysis of* $B \to K^*\ell^+\ell^-$, *Phys. Rev. Lett.* **118** (2017) 111801 [1612.05014].

[13] ATLAS collaboration, *Angular analysis of* $B_d^0 \to K^*\mu^+\mu^-$ *decays in pp collisions at* $\sqrt{s} = 8$ *TeV with the ATLAS detector*, *JHEP* **10** (2018) 047 [1805.04000].

[14] CMS collaboration, *Measurement of angular parameters from the decay* $B^0 \to K^{*0}\mu^+\mu^-$ *in proton-proton collisions at* $\sqrt{s} = 8$ *TeV*, *Phys. Lett.* **B781** (2018) 517 [1710.02846].

[15] J. Lyon and R. Zwicky, *Resonances gone topsy turvy - the charm of QCD or new physics in* $b \to s\ell^+\ell^-$ *?*, 1406.0566.

[16] C. Bobeth, U. Haisch, A. Lenz, B. Pecjak and G. Tetlalmatzi-Xolocotzi, *On new physics in* $\Delta\Gamma_d$, *JHEP* **06** (2014) 040 [1404.2531].

[17] J. Brod, A. Lenz, G. Tetlalmatzi-Xolocotzi and M. Wiebusch, *New physics effects in tree-level decays and the precision in the determination of the quark mixing angle γ*, *Phys. Rev.* **D92** (2015) 033002 [`1412.1446`].

[18] K. G. Chetyrkin, M. Misiak and M. Munz, *Weak radiative B meson decay beyond leading logarithms*, *Phys. Lett.* **B400** (1997) 206 [`hep-ph/9612313`].

[19] B. Grinstein, R. P. Springer and M. B. Wise, *Effective Hamiltonian for Weak Radiative B Meson Decay*, *Phys. Lett.* **B202** (1988) 138.

[20] B. Grinstein, R. P. Springer and M. B. Wise, *Strong Interaction Effects in Weak Radiative $\bar{B}$ Meson Decay*, *Nucl. Phys.* **B339** (1990) 269.

[21] M. Misiak, *QCD corrected effective Hamiltonian for the $b \to s$ gamma decay*, *Phys. Lett.* **B269** (1991) 161.

[22] CKMFITTER GROUP collaboration, *CP violation and the CKM matrix: Assessing the impact of the asymmetric B factories*, *Eur. Phys. J.* **C41** (2005) 1 [`hep-ph/0406184`].

[23] UTFIT collaboration, *The Unitarity Triangle Fit in the Standard Model and Hadronic Parameters from Lattice QCD: A Reappraisal after the Measurements of Δm_s and $BR(B \to \tau \nu_\tau)$*, *JHEP* **10** (2006) 081 [`hep-ph/0606167`].

[24] A. J. Buras, M. Misiak, M. Munz and S. Pokorski, *Theoretical uncertainties and phenomenological aspects of $B \to X_s \gamma$ decay*, *Nucl. Phys.* **B424** (1994) 374 [`hep-ph/9311345`].

[25] C. Greub, T. Hurth and D. Wyler, *Virtual $O(\alpha_s)$ corrections to the inclusive decay $b \to s\gamma$*, *Phys. Rev.* **D54** (1996) 3350 [`hep-ph/9603404`].

[26] A. J. Buras, M. Misiak and J. Urban, *Two loop QCD anomalous dimensions of flavor changing four quark operators within and beyond the standard model*, *Nucl. Phys.* **B586** (2000) 397 [`hep-ph/0005183`].

[27] P. Gambino, M. Gorbahn and U. Haisch, *Anomalous dimension matrix for radiative and rare semileptonic B decays up to three loops*, *Nucl. Phys.* **B673** (2003) 238 [`hep-ph/0306079`].

[28] C. Bobeth, P. Gambino, M. Gorbahn and U. Haisch, *Complete NNLO QCD analysis of $\bar{B} \to X_s \ell^+ \ell^-$ and higher order electroweak effects*, *JHEP* **04** (2004) 071 [`hep-ph/0312090`].

[29] A. Lenz, *Lifetimes and heavy quark expansion*, *Int. J. Mod. Phys.* **A30** (2015) 1543005 [`1405.3601`].

[30] M. Kirk, A. Lenz and T. Rauh, *Dimension-six matrix elements for meson mixing and lifetimes from sum rules*, *JHEP* **12** (2017) 068 [`1711.02100`].

[31] M. Beneke, G. Buchalla, C. Greub, A. Lenz and U. Nierste, *The $B^+ - B_d^0$ lifetime difference beyond leading logarithms*, *Nucl. Phys.* **B639** (2002) 389 [`hep-ph/0202106`].

[32] E. Franco, V. Lubicz, F. Mescia and C. Tarantino, *Lifetime ratios of beauty hadrons at the next-to-leading order in QCD*, *Nucl. Phys.* **B633** (2002) 212 [`hep-ph/0203089`].

[33] M. Artuso, G. Borissov and A. Lenz, *CP violation in the B_s^0 system*, *Rev. Mod. Phys.* **88** (2016) 045002 [`1511.09466`].

[34] M. Beneke, G. Buchalla, C. Greub, A. Lenz and U. Nierste, *Next-to-leading order QCD corrections to the lifetime difference of B_s mesons*, *Phys. Lett.* **B459** (1999) 631 [`hep-ph/9808385`].

[35] M. Beneke, G. Buchalla, A. Lenz and U. Nierste, *CP asymmetry in flavor specific B decays beyond leading logarithms*, *Phys. Lett.* **B576** (2003) 173 [`hep-ph/0307344`].

[36] M. Ciuchini, E. Franco, V. Lubicz, F. Mescia and C. Tarantino, *Lifetime differences and CP violation parameters of neutral B mesons at the next-to-leading order in QCD*, *JHEP* **08** (2003) 031 [`hep-ph/0308029`].

[37] A. Lenz and U. Nierste, *Theoretical update of $B_s - \bar{B}_s$ mixing*, *JHEP* **06** (2007) 072 [`hep-ph/0612167`].

[38] FERMILAB LATTICE, MILC collaboration, *$B^0_{(s)}$-mixing matrix elements from lattice QCD for the Standard Model and beyond*, *Phys. Rev.* **D93** (2016) 113016 [`1602.03560`].

[39] D. King, A. Lenz and T. Rauh, *B_s mixing observables and $|V_{td}/V_{ts}|$ from sum rules*, *JHEP* **05** (2019) 034 [`1904.00940`].

[40] R. J. Dowdall, C. T. H. Davies, R. R. Horgan, G. P. Lepage, C. J. Monahan, J. Shigemitsu et al., *Neutral B-meson mixing from full lattice QCD at the physical point*, `1907.01025`.

[41] M. Misiak et al., *Updated NNLO QCD predictions for the weak radiative B-meson decays*, *Phys. Rev. Lett.* **114** (2015) 221801 [`1503.01789`].

[42] HFLAV collaboration, *Averages of b-hadron, c-hadron, and τ-lepton properties as of summer 2016*, *Eur. Phys. J.* **C77** (2017) 895 [`1612.07233`].

[43] G. Buchalla, G. Isidori and S. J. Rey, *Corrections of order Λ^2_{QCD}/m^2_c to inclusive rare B decays*, *Nucl. Phys.* **B511** (1998) 594 [`hep-ph/9705253`].

[44] M. Benzke, S. J. Lee, M. Neubert and G. Paz, *Factorization at Subleading Power and Irreducible Uncertainties in $\bar{B} \to X_s\gamma$ Decay*, *JHEP* **08** (2010) 099 [`1003.5012`].

[45] M. Misiak and M. Steinhauser, *NNLO QCD corrections to the anti-B —> X(s) gamma matrix elements using interpolation in m(c)*, *Nucl. Phys.* **B764** (2007) 62 [`hep-ph/0609241`].

[46] P. Gambino and M. Misiak, *Quark mass effects in $\bar{B} \to X_s\gamma$*, *Nucl. Phys.* **B611** (2001) 338 [`hep-ph/0104034`].

[47] M. Beneke, T. Feldmann and D. Seidel, *Systematic approach to exclusive $B \to Vl^+l^-$, $V\gamma$ decays*, *Nucl. Phys.* **B612** (2001) 25 [`hep-ph/0106067`].

[48] PARTICLE DATA GROUP collaboration, *Review of Particle Physics*, *Phys. Rev.* **D98** (2018) 030001.

[49] M. Beneke, G. Buchalla, M. Neubert and C. T. Sachrajda, *QCD factorization for exclusive, nonleptonic B meson decays: General arguments and the case of heavy light final states*, *Nucl. Phys.* **B591** (2000) 313 [`hep-ph/0006124`].

[50] J. Chay and C. Kim, *Analysis of the QCD improved factorization in $B \to J/\psi K$*, `hep-ph/0009244`.

[51] H.-Y. Cheng and K.-C. Yang, *$B \to J/\psi K$ decays in QCD factorization*, *Phys. Rev.* **D63** (2001) 074011 [`hep-ph/0011179`].

[52] B. Melic, *Nonfactorizable corrections to $B \to J/\psi K$*, *Phys. Rev.* **D68** (2003) 034004 [`hep-ph/0303250`].

[53] K. G. Chetyrkin, J. H. Kuhn and M. Steinhauser, *RunDec: A Mathematica package for running and decoupling of the strong coupling and quark masses*, *Comput. Phys. Commun.* **133** (2000) 43 [`hep-ph/0004189`].

[54] F. Herren and M. Steinhauser, *Version 3 of RunDec and CRunDec*, *Comput. Phys. Commun.* **224** (2018) 333 [1703.03751].

[55] S. Aoki et al., *Review of lattice results concerning low-energy particle physics*, *Eur. Phys. J.* **C77** (2017) 112 [1607.00299].

[56] M. Czakon, P. Fiedler, T. Huber, M. Misiak, T. Schutzmeier and M. Steinhauser, *The $(Q_7, Q_{1,2})$ contribution to $\overline{B} \to X_s\gamma$ at $\mathcal{O}\left(\alpha_s^2\right)$*, *JHEP* **04** (2015) 168 [1503.01791].

[57] LHCв collaboration, *Test of lepton universality using $B^+ \to K^+\ell^+\ell^-$ decays*, *Phys. Rev. Lett.* **113** (2014) 151601 [1406.6482].

[58] LHCв collaboration, *Test of lepton universality with $B^0 \to K^{*0}\ell^+\ell^-$ decays*, *JHEP* **08** (2017) 055 [1705.05802].

[59] L.-S. Geng, B. Grinstein, S. Jäger, J. Martin Camalich, X.-L. Ren and R.-X. Shi, *Towards the discovery of new physics with lepton-universality ratios of $b \to s\ell\ell$ decays*, *Phys. Rev.* **D96** (2017) 093006 [1704.05446].

[60] M. Algueró, B. Capdevila, S. Descotes-Genon, P. Masjuan and J. Matias, *Are we overlooking lepton flavour universal new physics in $b \to s\ell\ell$?*, *Phys. Rev.* **D99** (2019) 075017 [1809.08447].

[61] M. Algueró, B. Capdevila, A. Crivellin, S. Descotes-Genon, P. Masjuan, J. Matias et al., *Emerging patterns of New Physics with and without Lepton Flavour Universal contributions*, 1903.09578.

[62] J. Aebischer, W. Altmannshofer, D. Guadagnoli, M. Reboud, P. Stangl and D. M. Straub, *B-decay discrepancies after Moriond 2019*, 1903.10434.

[63] A. Paul and D. M. Straub, *Constraints on new physics from radiative B decays*, *JHEP* **04** (2017) 027 [1608.02556].

[64] G. Bailas, B. Blossier and V. Morénas, *Some hadronic parameters of charmonia in $N_f = 2$ lattice QCD*, *Eur. Phys. J.* **C78** (2018) 1018 [1803.09673].

[65] D. Bečirević, G. Duplančić, B. Klajn, B. Melić and F. Sanfilippo, *Lattice QCD and QCD sum rule determination of the decay constants of η_c, J/ψ and h_c states*, *Nucl. Phys.* **B883** (2014) 306 [1312.2858].

[66] G. C. Donald, C. T. H. Davies, R. J. Dowdall, E. Follana, K. Hornbostel, J. Koponen et al., *Precision tests of the J/ψ from full lattice QCD: mass, leptonic width and radiative decay rate to η_c*, *Phys. Rev.* **D86** (2012) 094501 [1208.2855].

[67] A. Khodjamirian and A. V. Rusov, $B_s \to K\ell\nu_\ell$ and $B_{(s)} \to \pi(K)\ell^+\ell^-$ decays at large recoil and CKM matrix elements, *JHEP* **08** (2017) 112 [1703.04765].

[68] J. A. Bailey et al., $B \to Kl^+l^-$ *Decay Form Factors from Three-Flavor Lattice QCD*, *Phys. Rev.* **D93** (2016) 025026 [1509.06235].

[69] HPQCD collaboration, *Rare decay $B \to K\ell^+\ell^-$ form factors from lattice QCD*, *Phys. Rev.* **D88** (2013) 054509 [1306.2384].

[70] A. Lenz and G. Tetlalmatzi-Xolocotzi, "in preparation."

[71] R. Mertig, M. Bohm and A. Denner, *FEYN CALC: Computer algebraic calculation of Feynman amplitudes*, *Comput. Phys. Commun.* **64** (1991) 345.

[72] V. Shtabovenko, R. Mertig and F. Orellana, *New Developments in FeynCalc 9.0*, *Comput. Phys. Commun.* **207** (2016) 432 [1601.01167].